

Cyclin C promotes development and progression of B-cell acute lymphoblastic leukemia by counteracting p53-mediated stress responses

by Jana Trifinopoulos, Julia List, Thorsten Klampfl, Klara Klein, Michaela Prchal-Murphy, Agnieszka Witalisz-Siepracka, Florian Bellutti, Luca L. Fava, Gerwin Heller, Sarah Stummer, Patricia Testori, Monique L. den Boer, Judith M. Boer, Sonja Marinovic, Gregor Hoermann, Wencke Walter, Andreas Villunger, Piotr Sicinski, Veronika Sexl, and Dagmar Gotthardt

Received: April 18, 2024.

Accepted: September 30, 2024.

Citation: Jana Trifinopoulos, Julia List, Thorsten Klampfl, Klara Klein, Michaela Prchal-Murphy, Agnieszka Witalisz-Siepracka, Florian Bellutti, Luca L. Fava, Gerwin Heller, Sarah Stummer, Patricia Testori, Monique L. den Boer, Judith M. Boer, Sonja Marinovic, Gregor Hoermann, Wencke Walter, Andreas Villunger, Piotr Sicinski, Veronika Sexl, and Dagmar Gotthardt. Cyclin C promotes development and progression of B-cell acute lymphoblastic leukemia by counteracting p53-mediated stress responses.

Haematologica. 2024 Oct 10. doi: 10.3324/haematol.2024.285701 [Epub ahead of print]

Publisher's Disclaimer.

E-publishing ahead of print is increasingly important for the rapid dissemination of science. Haematologica is, therefore, E-publishing PDF files of an early version of manuscripts that have completed a regular peer review and have been accepted for publication.

E-publishing of this PDF file has been approved by the authors.

After having E-published Ahead of Print, manuscripts will then undergo technical and English editing, typesetting, proof correction and be presented for the authors' final approval; the final version of the manuscript will then appear in a regular issue of the journal.

All legal disclaimers that apply to the journal also pertain to this production process.

Cyclin C promotes development and progression of B-cell acute lymphoblastic leukemia by counteracting p53-mediated stress responses

Jana Trifinopoulos¹, Julia List¹, Thorsten Klampfl¹, Klara Klein¹, Michaela Prchal-Murphy¹, Agnieszka Witalisz-Siepracka^{1,2}, Florian Bellutti³, Luca L. Fava³, Gerwin Heller⁴, Sarah Stummer¹, Patricia Testori¹, Monique L. den Boer^{5,6}, Judith M. Boer⁵, Sonja Marinovic⁷, Gregor Hoermann⁸, Wencke Walter⁸, Andreas Villunger⁹, Piotr Sicinski¹⁰, Veronika Sexl^{1,11} and Dagmar Gotthardt^{1,*}

¹ Department for Biological Sciences and Pathobiology, University of Veterinary Medicine, Vienna, Austria.

² Department of Pharmacology, Physiology and Microbiology, Division Pharmacology, Karl Landsteiner University of Health Sciences, Krems, Austria.

³ Armenise-Harvard Laboratory of Cell Division, Department of Cellular, Computational and Integrative Biology - CIBIO, University of Trento, Trento, Italy.

⁴ Division of Oncology, Department of Medicine I, Medical University of Vienna, Vienna, Austria.

⁵ Princess Máxima Center for Pediatric Oncology, Utrecht, the Netherlands.

⁶ Erasmus MC-Sophia Children's Hospital, Rotterdam, the Netherlands.

⁷ Division of Molecular Medicine, Laboratory of Personalized Medicine, Ruder Boskovic Institute, Zagreb, Croatia.

⁸ MLL Munich Leukemia Laboratory, Munich, Germany.

⁹ Institute for Developmental Immunology, Biocenter, Medical University of Innsbruck, Innsbruck, Austria; Ludwig Boltzmann Institute for Rare and Undiagnosed Diseases (LBI-RUD), Vienna, Austria; CeMM Research Center for Molecular Medicine of the Austrian Academy of Sciences, Vienna, Austria.

¹⁰ Department of Cancer Biology, Dana-Farber Cancer Institute, Boston, MA, USA; Department of Genetics, Blavatnik Institute, Harvard Medical School, Boston, MA, USA.

¹¹ University of Innsbruck, Innsbruck, Austria.

Running head: Cyclin C in B-ALL

***Corresponding author:** Dagmar Gotthardt

Department for Biological Sciences and Pathobiology

University of Veterinary Medicine

Veterinärplatz 1, A-1210 Vienna, Austria

Phone number: +431 25077 2900

Email: dagmar.gotthardt@vetmeduni.ac.at

Data-sharing statement

The RNA-Seq data reported in this article have been deposited in the Array Express database

(Accession number: E-MTAB-13728). All other relevant data that support the conclusions of

the study are available from the authors on request. Please contact

dagmar.gotthardt@vetmeduni.ac.at

Authorship Contributions

J.T., V.S. and D.G. conceived the study; J.T., J.L., K.K., M.P.M., A.W.S, P.T., S.S., S.M., F.B. and D.G. performed the experiments. J.T., V.S. and D.G. analyzed the data. F.B. and M.P.M. provided help with the experiments and analysis of the data. L.L.F. and A.V. were involved in experimental design and scientific discussions; T.K. and J.T. analyzed sequencing data; G.Hoermann, W.W., J.M.B. and M.L.d.B. provided bioinformatic patient data analysis; G.Heller provided bioinformatic support and scientific input; F.B., M.P.M, and P.S. established methods; M.P.M and V.S. obtained the ethical permits for the experiments and oversaw ethical aspects. L.L.F., D.G. and V.S. provided reagents. D.G. and V.S. supervised the study; J.T. and D.G. wrote the manuscript and all authors revised the manuscript.

Disclosures

P.S. has been a consultant at Novartis, Genovis, Guidepoint, The Planning Shop, ORIC Pharmaceuticals, Cedilla Therapeutics, Syros Pharmaceuticals, Blueprint Medicines, Curie Bio, Differentiated Therapeutics, Excientia, Ligature Therapeutics, Merck, Redesign Science, Sibylla Biotech and Exo Therapeutics; his laboratory receives research funding from Novartis. G.Hoermann and W.W. are employed by MLL Munich Leukemia Laboratory.

Acknowledgements

We want to thank Sabine Fajmann, Petra Kudweis, Philipp Jodl, Alessia Mattivi and Michaela Ensfelder-Koperek for great technical support. We are indebted to our animal caretaker team. For valuable scientific discussions and conceptual input, we want to thank

Thomas Decker, Karl Kuchler, Birgit Strobl, Vanessa Maria Knab, Sebastian Kollmann and Andrea Hölbl.

Funding

This work was funded by the Austrian Science Fund (FWF) doc.funds DOC 32-B28 (grant DOI: 10.55776/DOC32), the Special Research Program SFB-F6107 (grant DOI: 10.55776/F61), the PhD program “Inflammation and Immunity” FWF W1212, the FWF ZK-81B (grant DOI: 10.55776/ZK81) and by R01CA269285 (to P.S.). K.K. was supported by a DOC Fellowship of the Austrian Academy of Sciences at the University of Veterinary Medicine. The L.L.F. lab is supported by AIRC (MFAG 2019 - ID 23560 project). For open access purposes, the author has applied a CC BY public copyright license to any author-accepted manuscript version arising from this submission. Additionally, the project was supported by the University of Veterinary Medicine Vienna.

Abstract

Despite major therapeutic advances in the treatment of acute lymphoblastic leukemia (ALL), resistances and long-term toxicities still pose significant challenges. Cyclins and their associated cyclin-dependent kinases are one focus of cancer research when looking for targeted therapies. We discovered cyclin C as a key factor for B-ALL development and maintenance. While cyclin C is non-essential for normal hematopoiesis, *Ccnc*^{Δ/Δ} BCR::ABL1⁺ B-ALL cells fail to elicit leukemia in mice. RNA sequencing experiments revealed a p53 pathway deregulation in *Ccnc*^{Δ/Δ} BCR::ABL1⁺ cells resulting in the incapability of the leukemic cells to adequately respond to stress. A genome-wide CRISPR/Cas9 loss-of-function screen supplemented with additional knock-outs unveiled a dependency of human B-lymphoid cell lines on *CCNC*. High cyclin C levels in B-cell precursor (BCP) ALL patients were associated with poor event-free survival and increased risk of early disease recurrence after remission.

Our findings highlight cyclin C as potential therapeutic target for B-ALL, particularly to enhance cancer cell sensitivity to stress and chemotherapy.

Introduction

The Philadelphia (Ph) chromosome, a product of the reciprocal translocation t(9;22)(q34;q11) between chromosomes 9 and 22, encodes the BCR::ABL1 fusion oncoprotein¹. The constitutively active BCR::ABL1 tyrosine kinase is a hallmark of chronic myeloid leukemia (CML) and drives a subset of acute lymphoblastic leukemia (ALL). The incidence of Ph positive (Ph+) ALL correlates with age, from only 3% in pediatric ALL to around 25% in older adults². Direct targeting of the BCR::ABL1 kinase with tyrosine kinase inhibitors (TKIs) has been a breakthrough in targeted cancer therapy. Despite efforts to counteract TKI resistance and improve safety profiles, refractory BCR::ABL1⁺ leukemia as well as toxicities and long-term side effects of TKIs present particular therapeutic challenges³⁻⁵.

The clinical relevance of cyclins and their associated cyclin-dependent kinases (CDKs) has been a major focus of research for several years. Cyclin-CDK complexes do not only drive the cell cycle, but are also important players in various other cellular processes including transcriptional and epigenetic regulation, metabolism or stem cell self-renewal⁶. In line with their importance in different pathways, cyclin-CDK complex dysregulation is implicated in many different types of cancer⁷.

Cyclin C belongs to the transcriptional cyclins, with its most notable role being the activating partner of the CDK8/19 serine/threonine kinases. Both CDK8 and cyclin C are essential for embryonic development as transgenic mice lacking either protein are not viable while deletion in adult mice is generally well tolerated⁸⁻¹⁰. The cyclin C-CDK8 kinase complex can regulate transcription by phosphorylation of different substrates including histone H3¹¹, the NOTCH intracellular domain^{8,12}, STAT transcription factors¹³, and SMAD proteins¹⁴.

In addition, cyclin C plays a transcriptional role as a member of the CDK8/19 kinase module (CKM) of the Mediator, a regulatory subunit that acts as modulator of the interaction between

the large Mediator complex and RNA Polymerase II and consists of MED12/12L, MED13/13L, CDK8/CDK19 and cyclin C¹⁵. Apart from its transcriptional function, some studies also report that cyclin C in complex with CDK1/2/3 has a role in cell cycle regulation^{8,16}. In addition, non-canonical functions of cyclin C in mitochondrial fragmentation have been elucidated which are separate from its binding to CDKs^{17,18}. The diverse pathways through which cyclin C operates might also account for its highly context-dependent role in cancer: in T-ALL and osteosarcoma it functions as a tumor suppressor^{8,19}. In thyroid tissue, cyclin C cooperates with PTEN to suppress cancer development²⁰. Conversely, *CCNC* amplification is associated with poor survival in colon adenocarcinoma²¹ and high *CCNC* levels correlate with poor relapse-free survival in breast cancer patients^{22,23}. Cyclin C-specific roles in B-cell malignancies have not been investigated yet.

Comprehending the mechanisms driving the progression of B-ALL is a fundamental prerequisite for developing innovative pharmacological inhibitors and refining treatment strategies. Within this study, we investigated the role of cyclin C in the development and maintenance of B-ALL and demonstrate its pivotal oncogenic role in leukemic cells both *in vitro* and *in vivo*.

Methods

Study approvals

All experiments were conducted with gender- and age-matched 6-12 week old mice in accordance with the Ethics and Animal Welfare Committee of the University of Veterinary Medicine Vienna and the national authority according to §26 Animal Experiments Act (Tierversuchsgesetz) 2012 (licence numbers BMWFV-68.205/0093-WF/V/3b/2015, 2022-0.404.452 and BMBWF-68.205/0174-V/3b/2018) and according to the guidelines of FELASA and ARRIVE.

Leukemia monitoring

To monitor leukemia development over time, gender- and age-matched 8-12 week old NOD *scid* gamma (NSG) mice were injected with 2.500 BCR::ABL1^{p185+} cells via the tail vein. Mice were monitored daily and sacrificed upon manifestation of disease symptoms (hindleg paralysis, hunched posture, decreased mobility, weight loss). Alternatively, leukemic cell infiltration at a specific time point was assessed by sacrificing the whole cohort of transplanted mice 26 days post-injection.

Patient data analysis

For comparison of *CCNC* levels in leukemia patients, the preparation of the RNA sequencing (RNA-Seq) libraries and the pre-processing of sequencing data was done as previously described at the MLL Munich Leukemia Laboratory²⁴. Bone marrow (BM) mononuclear cells from healthy donors served as controls. Raw counts were normalized by applying the Trimmed mean of M-values method from the edgeR package²⁵, producing log₂ CPM values.

To determine the event-free survival (EFS) probability for patients with high versus low *CCNC*-expressing B-cell precursor (BCP) ALL, expression levels were analyzed in a cohort of 573 pediatric BCP-ALL patients described by van der Veer *et al.*²⁶. Expression of *CCNC* at first diagnosis was determined with Affymetrix U133 plus2.0 gene expression microarrays using probeset 201955_at after vsnrma normalization²⁷. Expression data are published by Polak *et al.*²⁸ and have been deposited at GEO (accession number: GSE87070). As high/low cut-off for *CCNC* expression, median expression among BCP-ALL samples was used.

Results

Malignant B-lymphoblastic cells depend on cyclin C

To analyze the impact of deleting components of the cyclin C-CDK8/19 kinase complex, we queried the genome-wide CRISPR/Cas9-based loss-of-function screens performed for the

Cancer Dependency Map (DepMap) Project and investigated the effects of *CCNC*, *CDK8* or *CDK19* knock-out across a panel of 1095 human cancer cell lines (**Figure 1A**). Among these 1095 cell lines, 258 cell lines exhibited a dependency on cyclin C, whereas only 50 displayed a dependency on CDK8 and none were reliant on CDK19. Notably, the loss of *CCNC* had a pronounced impact on distinct cell lines, particularly those associated with plasma cell myelomas and cell lines of lymphoid origin, specifically B-lymphoblastic leukemia/lymphoma cell lines (**Figure 1B, Figure S1A**). The dependency of plasma cell myelomas on cyclin C was accompanied by a dependency on CDK8 while leukemic cells were not among the enriched lineages for CDK8 dependency (**Figure S1B**). This prompted us to investigate the role of cyclin C in the development and progression of B-cell leukemia and to validate its potential as novel therapeutic vulnerability.

Cyclin C is dispensable for normal hematopoiesis

We first studied the consequences of cyclin C deficiency for hematopoiesis and crossed conditional *Ccnc*^{fl/fl} mice⁸ with *VavCre*²⁹ mice. *Ccnc*^{fl/fl} *VavCre*^{-/-} (*Ccnc*^{fl/fl}) and *Ccnc*^{fl/fl} *VavCre*^{+/-} (*Ccnc*^{fl/fl} *VavCre*) mice were born at the expected Mendelian ratio (**Figure S2A**) and the ablation of cyclin C in BM and spleens of *Ccnc*^{fl/fl} *VavCre* mice was confirmed via immunoblotting (**Figure 2A**). Total cell counts in BM and spleen remained unchanged by *Ccnc* deletion (**Figure S2B**) and peripheral blood analysis indicated comparable numbers of white blood cells, red blood cells and platelets (**Figure S2C, D**). Flow cytometric analyses failed to detect any alterations of the numbers of Lin⁻Sca-1⁺c-kit⁺ (LSK) cells and progenitor cell subsets in *Ccnc*^{fl/fl} *VavCre* animals (**Figure 2B, C; Figure S2E, F**).

As the analysis of human cell lines indicated a role of cyclin C in malignancies of B-lymphoid origin, we conducted a detailed analysis of B-cell development in *Ccnc*^{fl/fl} *VavCre* mice. We failed to detect any alterations in B-cell developmental stages starting from

common lymphoid progenitors (CLPs) in the BM (**Figure 2D**; **Figure S2G**). In essence, cyclin C deficiency in the hematopoietic system is well tolerated.

Cyclin C plays a pivotal role in the oncogenic transformation and immortalization of BCR::ABL1^{p185+} B-ALL

To investigate the role of cyclin C in B-ALL development and maintenance, we focused on Ph+ leukemia which represents the most common chromosomal aberration in adult ALL patients³⁰ and utilized well-established murine models which reliably and specifically promote B-ALL development. A retroviral pMSCV-*Bcr-Abl1-p185*-IRES-eGFP construct was used to transform BM cells isolated from *Ccnc^{fl/fl}* and *Ccnc^{fl/fl} VavCre* mice. In contrast to CDK8 deficiency¹⁰, absence of cyclin C impaired the initial leukemic transformation as evidenced by a significantly reduced number of *Ccnc^{ΔΔ}* colonies derived from BM of *Ccnc^{fl/fl} VavCre* mice in growth factor-free methylcellulose (**Figure 3A**). Primary BM cultured in methylcellulose supplemented with interleukin-7 (IL-7) served as control and proved that cytokine-dependent colony growth of non-transformed cells is unaffected by cyclin C deletion (**Figure 3B**). Cancer progression is a multistep process which requires cancer cells to overcome intrinsic checkpoint mechanisms for tumorigenesis³¹. To test the potential for immortalization, individual clones were picked and the outgrowth of stable cell lines in FCS-supplemented medium was monitored. Cyclin C ablation significantly decreased the ability to form monoclonal cell lines indicative of its impact on immortalization (**Figure 3C**). To control the experimental setting, we also directly infected BM from *Ccnc^{fl/fl}* and *Ccnc^{fl/fl} VavCre* mice with pMSCV-*Bcr-Abl1-p185*-IRES-eGFP retrovirus prior to seeding in IL-7-supplemented medium. While this approach facilitates the simultaneous emergence of multiple transformed clones, ensuring the reliable establishment of immortalized, stable cell lines, we noted again a significant decrease of outgrowing cell lines in the absence of cyclin C. In contrast, all wildtype BM samples

successfully underwent immortalization upon transformation with the *BCR::ABL1^{p185}* oncogene (**Figure S3A, B**). Comparable results were obtained using the v-ABL^{p160} oncoprotein, a murine variant of *BCR::ABL1^{p185}* (**Figure S3C, D**). Cyclin C deficiency increased the apoptotic cell fractions during cell line establishment (in not yet stable cell lines), indicating elevated apoptosis might account for the reduced capability of *Ccnc^{Δ/Δ}* cells to immortalize (**Figure 3D**).

Cyclin C regulates stress responses in *BCR::ABL1^{p185+}* B-ALL cells

Deletion of cyclin C reduced the number of emerging stable cell lines (**Figure S3A, B**). The cyclin C deficient *BCR::ABL1^{p185+}* cell lines that managed to immortalize showed comparable oncogene levels as indicated by the mean fluorescence intensity (MFI) of the co-expressed GFP (**Figure S3E**). Absence of cyclin C in these cell lines had no impact on the expression of CDK8/19 (**Figure S3F**). All *Ccnc^{fl/fl}* and *Ccnc^{Δ/Δ}* *BCR::ABL1^{p185+}* cell lines stained positive for the pan B-cell markers B220 and CD19. While all cell lines of both genotypes lacked the expression of maturation markers IgM and IgD, CD43 expression was reduced in *Ccnc^{Δ/Δ}* *BCR::ABL1^{p185+}* cells suggesting a more differentiated developmental stage (**Figure S3G-I**). All immortalized, stable cell lines proliferated in FCS-supplemented medium, but we observed a slight, statistically significant growth defect upon cyclin C deletion (**Figure 3E**). Following initial studies in yeast, later reports underscored the importance of cyclin C in mammalian stress response^{8,17,32}. This prompted us to evaluate the impact of serum starvation on the stable *Ccnc^{Δ/Δ}* *BCR::ABL1^{p185+}* cell lines. Nutrient deprivation for 24 hours led to an increase in the sub-G1 fraction that was more pronounced in cyclin C deficient cells indicating a role of cyclin C in stress response regulation of leukemic cells (**Figure 3F**).

Cyclin C deficiency impairs *in vivo* leukemia establishment

To test the disease-initiating potential of the cyclin C deficient cell lines *in vivo*, we transplanted $Ccnc^{fl/fl}$ and $Ccnc^{\Delta/\Delta}$ leukemic cells into NSG mice (**Figure 4A**). The severe immunodeficiency of these animals enables studying tumor-intrinsic properties of BCR::ABL1^{p185+} B-ALL *in vivo*. Wildtype BCR::ABL1^{p185+} cells initiated an aggressive leukemia and infiltrated BM, spleen and blood of the recipient mice within 26 days. In contrast, $Ccnc^{\Delta/\Delta}$ cells failed to elicit disease in the injected animals 26 days post-transplantation despite being still detectable at low numbers (**Figure 4B, C; Figure S4A-C**). This prompted us to monitor disease progression over time in a second independent experiment (**Figure 4D**). NSG mice injected with wildtype BCR::ABL1^{p185+} cells rapidly developed leukemia within 3-5 weeks, while $Ccnc^{\Delta/\Delta}$ cells with one exception did not elicit a disease over the period of 40 weeks. One animal from the $Ccnc^{\Delta/\Delta}$ cohort developed a B-ALL after 54 days (**Figure 4E**). The experiment was terminated after 281 days; at that time point no disease symptoms were detectable in the remaining $Ccnc^{\Delta/\Delta}$ BCR::ABL1^{p185+}-injected mice (**Figure 4F; Figure S4D-F**).

Cyclin C represses p53 responses in transformed cells

To understand how cyclin C interferes with BCR::ABL1-induced transformation, we performed RNA-Seq using *in vitro* cultured $Ccnc^{fl/fl}$ and $Ccnc^{\Delta/\Delta}$ BCR::ABL1^{p185+} cell lines. In addition, the cells were injected into NSG mice to allow adaption to the *in vivo* microenvironment. $Ccnc^{fl/fl}$ or $Ccnc^{\Delta/\Delta}$ BCR::ABL1^{p185+} cells were injected in high amounts (5×10^5 cells compared to 2,500 cells for disease initiation) which facilitated retrieval of sufficient numbers of $Ccnc^{\Delta/\Delta}$ cells from the BM ten days post-transplantation despite their reduced infiltration compared to control cells (**Figure 4; Figure 5A; Figure S5A**).

In vitro, cyclin C deficiency affected the transcription of 446 genes - 146 upregulated and 300 downregulated. In contrast, differential gene expression analysis from the *ex vivo* derived

samples showed profound transcriptional changes with 3179 deregulated genes in *Ccnc*^{Δ/Δ} cell lines compared to *ex vivo* controls - 1465 genes were upregulated and 1714 downregulated (**Figure 5B; Figure S5B, C**). Gene set enrichment analysis (GSEA) revealed 27 altered pathways in the *ex vivo* samples, of which nine were also deregulated *in vitro* such as interferon responses or Myc targets (**Figure S5D**). Among the pathways which were exclusively upregulated in *Ccnc*^{Δ/Δ} BCR::ABL1^{p185+} cells *ex vivo* were the apoptosis and the p53 pathways (**Figure 5C**). Notably, enhanced expression of the p53 targets *Plk*, *Sfn* and *Gadd45a* contributed significantly to the enrichment of the p53 pathway *ex vivo* (**Table S1**). GADD45a serves as an anti-oncogenic stress sensor in transformed cells and can inhibit the CDK1/cyclin B1 complex together with p21 and 14-3-3σ (encoded by *Sfn*)^{33,34}. The polo-like kinase PLK2 (SNK) likewise plays a role in stress signaling and has been described as tumor suppressor in B-cell malignancies^{35,36}. As the p53 gene set was not among the significantly enriched pathways in the *in vitro* samples, we subjected *in vitro* cultured cells to stress by reducing FCS or cell density. Inducing stress *in vitro* via serum starvation or sparse seeding inhibited the proliferation of *Ccnc*^{Δ/Δ} BCR::ABL1^{p185+} cells and enhanced the upregulation of several p53 pathway members including GADD45a, PLK2 and 14-3-3σ in cyclin C deficient cells (**Figure 5D, E; Figure S5E**). Upregulation of *Cdkn2b*, encoding the tumor suppressor p15^{INK4b}, which likewise contributed to the enrichment of the p53 pathway, could also be confirmed via RT-qPCR (**Figure S5E**). Notably, the enhanced expression of these p53 pathway genes *in vitro* only reached significance after provoking a stress response in *Ccnc*^{Δ/Δ} BCR::ABL1^{p185+} cells. In addition, the p53 target *Cdkn1a* encoding p21 was significantly upregulated *in vitro* in the *Ccnc*^{Δ/Δ} cell lines on mRNA as well as on protein level (**Figure S5F, G**), although no upregulation was observed in the *ex vivo* samples on mRNA level. The tumor suppressors p16^{INK4a} and p19^{ARF}, both encoded by the *Cdkn2a* gene, are also members

of the p53 pathway and upregulated in *Ccnc*^{Δ/Δ} BCR::ABL1^{p185+} cells in accordance with the RNA-Seq data (**Figure S5H**).

Disruption of functional p53 signaling restores the leukemogenicity of cyclin C deficient BCR::ABL1^{p185+} cells

As reducing cell density or serum concentrations *in vitro* increased the overexpression of the p53 pathway genes *Plk2*, *Sfn* and *Gadd45a* in *Ccnc*^{Δ/Δ} BCR::ABL1^{p185+} cells, we employed CRISPR/Cas9 to test the effects of silencing the genes under the same stressors. Individually depleting either of these p53 targets partially rescued the impaired proliferation of *Ccnc*^{Δ/Δ} cell lines, most pronouncedly under sparse seeding conditions (**Figure 6A**; **Figure S6A**). Since our data suggest that cyclin C deletion amplifies overall p53 responses in BCR::ABL1^{p185+} cells, we hypothesized that cumulative effects of aberrant p53 signaling might account for the distinct disease-initiating potential observed in one *Ccnc*^{Δ/Δ} cell line (**Figure 4E**, highlighted turquoise). Sanger sequencing analysis of *ex vivo* derived spleen-infiltrating BCR::ABL1^{p185+} cells from the single mouse in the *Ccnc*^{Δ/Δ} cohort which succumbed to leukemia revealed a *Tp53* mutation accompanied by accumulation of mutant p53 protein (**Figure 6B**), potentially counteracting the cyclin C deficiency and resulting in an aggressive disease phenotype. Analyses of spleens from mice injected with *Ccnc*^{fl/fl} BCR::ABL1^{p185+} cells revealed either wildtype or mutant p53, proving that in the presence of cyclin C, BCR::ABL1^{p185+} cells are able to elicit leukemia irrespective of *Tp53* mutational status.

To determine if functional loss of p53 signaling indeed restores the leukemogenicity of *Ccnc*^{Δ/Δ} BCR::ABL1^{p185+} cells *in vivo*, we screened for *Ccnc*^{Δ/Δ} cell lines carrying spontaneous *Tp53* mutations, injected them into NSG mice and monitored disease progression. Unlike *Ccnc*^{Δ/Δ} BCR::ABL1^{p185+} cells with intact p53 (**Figure 4E**),

BCR::ABL1^{p185+} cells lacking functional p53 rapidly caused a fatal B-ALL despite loss of cyclin C (**Figure 6C; Figure S6B**). In addition, inhibiting p53 by expressing dominant negative p53 (dn p53) in parental BCR::ABL1^{p185+} cells without spontaneous *Tp53* mutations (**Figure S6C**) restored the disease-initiating potential of *Ccnc*^{ΔΔ} B-ALL cells (**Figure 6D; Figure S6D**). These data indicate that enhanced p53 activity in cyclin C deficient BCR::ABL1^{p185+} cells could mechanistically explain their incapability to give rise to B-ALL *in vivo*.

Cyclin C as a potential new target for B-ALL treatment

To mimic a therapeutic setting and to target cyclin C in already transformed leukemic cells, we generated BCR::ABL1^{p185+} cell lines using BM from *Ccnc*^{fl/fl} *Mx1Cre* mice. Here, an interferon-responsive *Mx1* promoter allows Cre-mediated activation and excision of *Ccnc* upon interferon treatment/induction (**Figure S7A**). Deletion of cyclin C via treatment with interferon-beta (Ifn-β) inhibited leukemic cell proliferation *in vitro* (**Figure S7B**).

We next conducted a thorough analysis of RNA-Seq data from leukemia patients, revealing elevated *CCNC* levels in different hematological malignancies, including BCP-ALL (**Figure S7C**). Further examination of different BCP-ALL subtypes showed that cyclin C is overexpressed in all studied subclasses (**Figure 7A**). Notably, there was no upregulation observed in myeloid leukemia patient samples and cell lines of myeloid origin were not among the significantly enriched lineages for *CCNC* in the DepMap CRISPR/Cas9 knock-out screen (**Figure 1B**). To confirm this, we performed a colony formation assay using the *BCR::ABL1*^{p210} oncogene, detecting no significant differences in myeloid colony growth and affirming no dependency on cyclin C in CML (**Figure S7D**). Conversely, 5 out of 6 Ph-human B-lymphoblastic cell lines with intact p53 analyzed in the DepMap screen exhibited a dependency on *CCNC* (**Figure 7B**).

Subsequently, we employed CRISPR/Cas9 to target *CCNC* in the Ph- human BCP-ALL cell line NALM-6. This resulted in a notable reduction of outgrowing single cell clones with guide RNA #1 and #2 (**Figure 7C, D**). Despite an initial cyclin C reduction in the bulk cell culture, we were unable to generate cyclin C knock-out single cell clones after screening over 100 clones from three individual approaches. Moreover, continuous culture of the bulk cells following the knock-out approach resulted in the outgrowth of wildtype cells. This indicates that B-ALL cell lines are not compatible with cyclin C deficiency, and the few remaining clones that survive the initial knock-out have a proliferation or survival disadvantage.

To further assess the impact of cyclin C levels on disease outcome in human patients, we compared the EFS of pediatric BCP-ALL patients with high versus low *CCNC* expression. Above-median *CCNC* levels were associated with a significantly decreased EFS probability (**Figure 7E**). High *CCNC* expression was particularly associated with early relapse/death in patients who had already reached remission after induction therapy (**Figure 7F**).

In summary, our data show that cyclin C is important for the transformation and maintenance of BCR::ABL1^{p185+} leukemia and cyclin C-deficiency precludes leukemia development *in vivo*. This is in line with our analysis of human data sets showing a reliance of B-cell malignancies on cyclin C and increased risk of disease recurrence in BCP-ALL patients with high levels of *CCNC*.

Discussion

Cyclin C is a multifaceted protein with functions in transcriptional regulation and mitochondrial fragmentation. Its impact on oncogenesis is intricate and context-dependent. Found on chromosome 6q21, a segment frequently deleted in cancer³⁷, cyclin C may act as tumor suppressor or promoter. We here add a novel angle to the story by showing that in Ph+ B-ALL, cyclin C acts as an oncogene by suppressing p53 responses.

Cyclin C deficient BCR::ABL1⁺ cells lines can be established *in vitro*, albeit to a lesser extent, but are incapable of eliciting disease *in vivo*, which indicates a function of cyclin C in cellular adaptation and reaction to environmental stress. Similar to its oncogenic role, cyclin C's involvement in regulating stress response seems highly fine-tuned to the type of cell and stressor, influencing signaling pathways for either cell death or survival. Absence of cyclin C inhibits stress-mediated mitochondrial fission and cell death responses in yeast and mouse embryonic fibroblast (MEF) cells^{17,38}. On the other hand, studies in yeast have highlighted cyclin C's degradation via the ubiquitin-proteasome system following unfavorable environmental cues prior to nuclear release, thereby eliciting survival signals³⁹. In MEF cells, oxidative stress or mTOR inhibition cause distinct changes in CKM promoter occupancy to fine-tune the transcriptional stress response³². Adding another layer of complexity, cyclin C has been reported to play a role at different stages of the cell cycle by phosphorylating Rb and regulating E2F-dependent transcription factor activity^{8,16,40}. There is limited data available on the regulation of cyclin C expression itself, except that it is induced by various mitogenic signals such as vitamin D and IL-3^{41,42}.

We now show that cyclin C is vital for leukemic transformation and stress-adaptive responses in B-ALL. Cyclin C deficient BCR::ABL1⁺ cells display restricted transformation and immortalization. The outgrowth of fewer transformed clones suggests the presence of compensatory mechanisms in the surviving *Ccnc*^{Δ/Δ} BCR::ABL1^{p185+} cells, which could be explored in future studies. Nonetheless, these cyclin C deficient cells continue to display impaired stress adaptation even in their already transformed state (e.g., serum starvation, low cell density and upon transfer into immunocompromised mice). This concept is supported by the RNA-Seq results showing a significant upregulation of the p53 and apoptosis pathways in *Ccnc*^{Δ/Δ} BCR::ABL1^{p185+} cells *in vivo*. The importance of the p53 pathway in stress responses is well established. Upon sensing stress, p53 regulates the expression of genes involved in

diverse cellular processes, including DNA repair, cell cycle arrest and apoptosis, and prevents the propagation of damaged or compromised cells that could contribute to tumorigenesis or other abnormalities⁴³. GADD45a and PLK2, amongst our top hits in the p53 pathway, are known anti-oncogenic stress sensors^{33,35,36}. *In vitro*, their increased expression in *Ccnc*^{Δ/Δ} BCR::ABL1^{p185+} cells was not as pronounced as *in vivo*, possibly masked by optimal growth conditions. However, after introducing additional stress through a cell density or nutrient reduction *in vitro*, cyclin C ablation again caused significantly enhanced expression of the p53 pathway genes. The upregulation of several p53 pathway genes was also validated at the protein level. Their significance was further demonstrated by knock-out experiments, showing that loss of individual p53 targets partially rescued the impaired proliferation of cyclin C deficient leukemic cells under stress. The enhanced p53 activity observed in *Ccnc*^{Δ/Δ} BCR::ABL1^{p185+} cells under stress could thus at least partly explain why cyclin C deficiency is particularly harmful for leukemic cells during early transformation and in the absence of optimal growth conditions.

Disruption of the p53 pathway through a genomic *Tp53* mutation or via introduction of dn p53 restored the leukemic potential of *Ccnc*^{Δ/Δ} BCR::ABL1^{p185+} cells. While p53 mutations are more common in many solid tumors, aberrations of *TP53* in B-ALL increase with age and upon relapse and are associated with poor prognosis^{44,45}.

Based on our findings, cyclin C emerges as a potential new therapeutic target for B-ALL. While transformation and mechanistic studies were only conducted in BCR::ABL1^{p185+} cell lines, we also provide supporting evidence that cyclin C plays an essential role for Ph- B-ALL (**Figure 1** and **Figure 7**), suggesting that our findings are broadly relevant to B-ALL. Cyclin C's essential role in B-ALL, but not in normal B-cell development, may stem from its overexpression and critical involvement in promoting oncogene-driven proliferation and survival in leukemic cells. This dependency creates synthetic lethal vulnerabilities which

might be therapeutically exploited, offering a promising avenue for selectively targeting B-ALL cells. However, targeting molecules like cyclin C, given their intracellular location, lack of kinase activity, and complex protein interactions, has been challenging. Additionally, caution is needed due to potential detrimental effects on the heart⁴⁶. Proteolysis-targeting chimeras (PROTAC) are small molecule compounds that can selectively degrade previously undruggable molecules. PROTACS offer high specificity and strategies to additionally increase their safety profile include selective, cell-type-specific PROTAC delivery using nanoparticle delivery systems or antibody-PROTAC conjugates which could enable B-cell-specific targeting⁴⁷.

Loss of cyclin C renders B-ALL cells more vulnerable to stress, suggesting it as an interesting target for combination therapies as it may allow sensitization of cancer cells to, e.g., chemotherapy or radiotherapy. *In silico* analysis of pediatric BCP-ALL patients supports this notion: cyclin C expression is associated with decreased EFS and high *CCNC* levels show a particularly strong correlation with early disease recurrence in systematically treated patients. This suggests that cyclin C could compromise the prolonged efficacy of systemic therapy in patients who have achieved remission, and that additional targeting of cyclin C might provide synergistic effects. Successful cyclin-degrading compounds have been previously developed and tested^{48,49}. Developing degraders specifically targeting cyclin C and further studying its role in various tumor entities is therefore of high interest.

References

1. Groffen J, Stephenson JR, Heisterkamp N, de Klein A, Bartram CR, Grosveld G. Philadelphia chromosomal breakpoints are clustered within a limited region, bcr, on chromosome 22. *Cell*. 1984;36(1):93-99.
2. Pui CH, Jeha S. New therapeutic strategies for the treatment of acute lymphoblastic leukaemia. *Nat Rev Drug Discov*. 2007;6(2):149-165.
3. Quintás-Cardama A, Kantarjian H, Cortes J. Flying under the radar: The new wave of BCR-ABL inhibitors. *Nat Rev Drug Discov*. 2007;6(10):834-848.
4. Lee H, Basso IN, Kim DDH. Target spectrum of the BCR-ABL tyrosine kinase inhibitors in chronic myeloid leukemia. *Int J Hematol*. 2021;113(5):632-641.
5. Yang K, Fu L-W. Mechanisms of resistance to BCR-ABL TKIs and the therapeutic strategies: A review. *Crit Rev Oncol Hematol*. 2015;93(3):277-292.
6. Lim S, Kaldis P. Cdks, cyclins and CKIs: Roles beyond cell cycle regulation. *Development*. 2013;140(15):3079-3093.
7. Asghar U, Witkiewicz AK, Turner NC, Knudsen ES. The history and future of targeting cyclin-dependent kinases in cancer therapy. *Nat Rev Drug Discov*. 2015;14(2):130-146.
8. Li N, Fassl A, Chick J, et al. Cyclin C is a haploinsufficient tumour suppressor. *Nat Cell Biol*. 2014;16(11):1080-1091.
9. Westerling T, Kuuluvainen E, Mäkelä TP. Cdk8 Is Essential for Preimplantation

- Mouse Development. *Mol Cell Biol.* 2007;27(17):6177-6182.
10. Menzl I, Zhang T, Berger-Becvar A, et al. A kinase-independent role for CDK8 in BCR-ABL1+ leukemia. *Nat Commun.* 2019;10(1):4741.
 11. Meyer KD, Donner AJ, Knuesel MT, York AG, Espinosa JM, Taatjes DJ. Cooperative activity of cdk8 and GCN5L within Mediator directs tandem phosphoacetylation of histone H3. *EMBO J.* 2008;27(10):1447-1457.
 12. Fryer CJ, White JB, Jones KA. Mastermind recruits CycC:CDK8 to phosphorylate the Notch ICD and coordinate activation with turnover. *Mol Cell.* 2004;16(4):509-520.
 13. Bancerek J, Poss ZC, Steinparzer I, et al. CDK8 Kinase Phosphorylates Transcription Factor STAT1 to Selectively Regulate the Interferon Response. *Immunity.* 2013;38(2):250-262.
 14. Alarcón C, Zaromytidou AI, Xi Q, et al. Nuclear CDKs Drive Smad Transcriptional Activation and Turnover in BMP and TGF- β Pathways. *Cell.* 2009;139(4):757-769.
 15. Soutourina J. Transcription regulation by the Mediator complex. *Nat Rev Mol Cell Biol.* 2018;19(4):262-274.
 16. Ren S, Rollins BJ. Cyclin C/Cdk3 promotes Rb-dependent G0 exit. *Cell.* 2004;117(2):239-251.
 17. Wang K, Yan R, Cooper KF, Strich R. Cyclin C mediates stress-induced mitochondrial fission and apoptosis. *Mol Biol Cell.* 2015;26(6):1030-1043.
 18. Jezek J, Chang K, Joshi AM, Strich R. Mitochondrial translocation of cyclin C stimulates intrinsic apoptosis through Bax recruitment. *EMBO Rep.*

2019;20(9):e47425.

19. Ohata N, Ito S, Yoshida A, et al. Highly frequent allelic loss of chromosome 6q16-23 in osteosarcoma: Involvement of cyclin C in osteosarcoma. *Int J Mol Med*. 2006;18(6):1153-1158.
20. Jezek J, Wang K, Yan R, Di Cristofano A, Cooper KF, Strich R. Synergistic repression of thyroid hyperplasia by cyclin C and Pten. *J Cell Sci*. 2019;132(6):jcs230029.
21. Bondi J, Husdal A, Bukholm G, Nesland JM, Bakka A, Bukholm IRK. Expression and gene amplification of primary (A, B1, D1, D3, and E) and secondary (C and H) cyclins in colon adenocarcinomas and correlation with patient outcome. *J Clin Pathol*. 2005;58(5):509-514.
22. Broude E, Gyorffy B, Chumanevich A, et al. Expression of CDK8 and CDK8-interacting Genes as Potential Biomarkers in Breast Cancer. *Curr Cancer Drug Targets*. 2015;15(8):739-749.
23. Porter DC, Farmaki E, Altiglia S, et al. Cyclin-dependent kinase 8 mediates chemotherapy-induced tumor-promoting paracrine activities. *Proc Natl Acad Sci*. 2012;109(34):13799-13804.
24. Walter W, Shahswar R, Stengel A, et al. Clinical application of whole transcriptome sequencing for the classification of patients with acute lymphoblastic leukemia. *BMC Cancer*. 2021;21(1):886.
25. Robinson MD, Oshlack A. A scaling normalization method for differential expression analysis of RNA-seq data. *Genome Biol*. 2010;11(3):R25.
26. van der Veer A, Waanders E, Pieters R, et al. Independent prognostic value of BCR-

- ABL1-like signature and IKZF1 deletion, but not high CRLF2 expression, in children with B-cell precursor ALL. *Blood*. 2013;122(15):2622-2629.
27. Huber W, von Heydebreck A, Sültmann H, Poustka A, Vingron M. Variance stabilization applied to microarray data calibration and to the quantification of differential expression. *Bioinformatics*. 2002;18(Suppl 1):S96-S104.
 28. Polak R, Bierings MB, van der Leije CS, et al. Autophagy inhibition as a potential future targeted therapy for ETV6-RUNX1-driven B-cell precursor acute lymphoblastic leukemia. *Haematologica*. 2019;104(4):738-748.
 29. Georgiades P, Ogilvy S, Duval H, et al. VavCre transgenic mice: a tool for mutagenesis in hematopoietic and endothelial lineages. *Genesis*. 2002;34(4):251-256.
 30. Mrózek K, Harper DP, Aplan PD. Cytogenetics and Molecular Genetics of Acute Lymphoblastic Leukemia. *Hematol Oncol Clin North Am*. 2009;23(5):991-1010.
 31. Hanahan D, Weinberg RA. Hallmarks of cancer: The next generation. *Cell*. 2011;144(5):646-674.
 32. Stieg DC, Cooper KF, Strich R. The extent of cyclin C promoter occupancy directs changes in stress-dependent transcription. *J Biol Chem*. 2020;295(48):16280-16291.
 33. Liebermann DA, Tront JS, Sha X, Mukherjee K, Alisha-Mohamed-Hadley, Hoffman B. Gadd45 stress sensors in malignancy and leukemia. *Crit Rev Oncog*. 2011;16(1-2):129-140.
 34. Rizzotto D, Englmaier L, Villunger A. At a Crossroads to Cancer: How p53-Induced Cell Fate Decisions Secure Genome Integrity. *Int J Mol Sci*. 2021;22(19):10883.

35. Eckerdt F, Yuan J, Strebhardt K. Polo-like kinases and oncogenesis. *Oncogene*. 2005;24(2):267-276.
36. Syed N, Smith P, Sullivan A, et al. Transcriptional silencing of Polo-like kinase 2 (SNK/PLK2) is a frequent event in B-cell malignancies. *Blood*. 2006;107(1):250-256.
37. Li H, Lahti JM, Valentine M, et al. Molecular cloning and chromosomal localization of the human cyclin C (CCNC) and cyclin E (CCNE) genes: Deletion of the CCNC gene in human tumors. *Genomics*. 1996;32(2):253-259.
38. Strich R, Cooper KF. The dual role of cyclin C connects stress regulated gene expression to mitochondrial dynamics. *Microb Cell*. 2014;1(10):318-324.
39. Willis SD, Hanley SE, Beishke T, Tati PD, Cooper KF. Ubiquitin–proteasome-mediated cyclin C degradation promotes cell survival following nitrogen starvation. *Mol Biol Cell*. 2020;31(10):1015-1031.
40. Trakala M, Malumbres M. Cyclin C surprises in tumour suppression. *Nat Cell Biol*. 2014;16(11):1031-1033.
41. Sinkkonen L, Malinen M, Saavalainen K, Väisänen S, Carlberg C. Regulation of the human cyclin C gene via multiple vitamin D₃-responsive regions in its promoter. *Nucleic Acids Res*. 2005;33(8):2440-2451.
42. Liu Z-J, Ueda T, Miyazaki T, et al. A Critical Role for Cyclin C in Promotion of the Hematopoietic Cell Cycle by Cooperation with c-Myc. *Mol Cell Biol*. 1998;18(6):3445-3454.
43. Oren M. Decision making by p53: Life, death and cancer. *Cell Death Differ*. 2003;10(4):431-442.

44. Salmoiraghi S, Montalvo MLG, Ubiali G, et al. Mutations of TP53 gene in adult acute lymphoblastic leukemia at diagnosis do not affect the achievement of hematologic response but correlate with early relapse and very poor survival. *Haematologica*. 2016;101(6):e245-e248.
45. Stengel A, Schnittger S, Weissmann S, et al. TP53 mutations occur in 15.7% of ALL and are associated with MYC-rearrangement, low hypodiploidy, and a poor prognosis. *Blood*. 2014;124(2):251-258.
46. Ponce JM, Coen G, Spitler KM, et al. Stress-induced cyclin c translocation regulates cardiac mitochondrial dynamics. *J Am Heart Assoc*. 2020;9(7):e014366.
47. Békés M, Langley DR, Crews CM. PROTAC targeted protein degraders: the past is prologue. *Nat Rev Drug Discov*. 2022;21(3):181-200.
48. Mayor-Ruiz C, Bauer S, Brand M, et al. Rational discovery of molecular glue degraders via scalable chemical profiling. *Nat Chem Biol*. 2020;16(11):1199-1207.
49. Li J, Liu T, Song Y, et al. Discovery of Small-Molecule Degradors of the CDK9-Cyclin T1 Complex for Targeting Transcriptional Addiction in Prostate Cancer. *J Med Chem*. 2022;65(16):11034-11057.

Figure Legends

Figure 1. Malignant B-lymphoblastic cells depend on cyclin C. (A) CRISPR dependencies for *CCNC*, *CDK8* and *CDK19* in a panel of human cancer cell lines obtained from the Broad Institute Cancer Dependency Map (DepMap). The dots correspond to individual cell lines (n = 1095), the y-axis represents the CRISPR dependency score (DepMap Public 23Q2+Score, Chronos). Negative gene effect scores imply dependency of a cell line on a given gene as gene knock-out results in impaired cell line growth and/or death. Scores are normalized so that all nonessential genes have a median score of 0 and all common essential genes have a median score of -1. Cell lines with probability of dependency greater than 0.5 are considered dependent. (B) Representation of the top 8 significantly enriched lineages (p<0.0005, t-test) in the Depmap CRISPR dependency screen for *CCNC*. The number of cell lines included in each lineage subset is denoted in parentheses. Ranking was done based on effect size.

Figure 2. Cyclin C is dispensable for normal hematopoiesis. (A) (Left) Breeding scheme for the generation of *Ccnc*^{fl/fl} *VavCre*^{-/-} (*Ccnc*^{fl/fl}) and *Ccnc*^{fl/fl} *VavCre*^{+/-} (*Ccnc*^{fl/fl} *VavCre*) mice. (Right) Cyclin C immunoblot analysis of BM and spleen from *Ccnc*^{fl/fl} and *Ccnc*^{fl/fl} *VavCre* mice (n=3 per genotype). HSC70 served as loading control. (B) Lin⁻Sca-1⁺c-kit⁺ (LSK) frequencies in BM of *Ccnc*^{fl/fl} (n = 12) and *Ccnc*^{fl/fl} *VavCre* (n = 11) mice, one representative out of two independent experiments is shown. (C) Relative fold change of BM subpopulations from *Ccnc*^{fl/fl} *VavCre* normalized to the mean value from *Ccnc*^{fl/fl} mice (n = 9-12). (D) (Left) Representative flow cytometry plots depicting the gating scheme for early B-cell development populations according to expression of the markers CD43, B220, BP-1, CD19, IgM, IgD and (right) summary of frequencies in the BM of *Ccnc*^{fl/fl} (n = 12) and *Ccnc*^{fl/fl} *VavCre* (n = 10) mice normalized to mean values from *Ccnc*^{fl/fl} mice. Details on flow cytometric analyses are provided in the *Supplementary Materials and Methods*. Bar graphs represent mean ± SD. Box and whiskers plot center values represent median, the box 25th to 75th percentiles, and whiskers min to max. Levels of significance were calculated using (B-D) Mann-Whitney U-test. Abbreviations: BM, bone marrow; HSC, hematopoietic stem cells; MPP, multipotent progenitor population; CLP, common lymphoid progenitors

Figure 3. Cyclin C plays a pivotal role in the oncogenic transformation and immortalization of BCR::ABL1^{p185+} B-ALL. BM cells from *Ccnc*^{fl/fl} and *Ccnc*^{fl/fl} *VavCre* mice were isolated and either (A) infected with a retrovirus encoding BCR::ABL1^{p185} prior to plating in growth-factor free methylcellulose or (B) directly plated in methylcellulose containing IL-7. Pictures show individual colonies for each genotype. The number of colonies (colony forming units (CFU)) were counted and are depicted normalized to mean values from *Ccnc*^{fl/fl} mice. ((A) n =12 per genotype, pooled from four independent experiments, performed in technical duplicates (B) n=3 per genotype, performed in technical duplicates, one representative result from two experimental set-ups with different concentrations of plated BM cells is shown). (C) Statistics on the percentage of immortalized monoclonal cell lines proliferating in FCS-supplemented medium after picking individual colonies from a BCR::ABL1^{p185}-induced colony formation assay (n = 14-30 picked colonies/genotype). Error bars represent confidence intervals calculated using the Wilson Score interval (95% confidence level). (D-F) BM cells from *Ccnc*^{fl/fl} and *Ccnc*^{fl/fl} *VavCre* mice were isolated, transformed with a pMSCV-*Bcr-Abl1-p185*-IRES-eGFP-based retrovirus and cultured in liquid medium to monitor outgrowth. (D) Bar graphs summarizing the result of Annexin/7-AAD stainings performed 6 weeks after transformation of BM of *Ccnc*^{fl/fl} and *Ccnc*^{fl/fl} *VavCre* mice with the BCR::ABL1^{p185} oncogene. Depicted are frequencies of living (Annexin⁻ 7-AAD⁻), early apoptotic (Annexin⁺ 7-AAD⁻) and late apoptotic/necrotic (Annexin⁺ 7-AAD⁺) fractions from n=6-8 biological replicates/genotype. (E) Growth curves of stable *Ccnc*^{fl/fl} and *Ccnc*^{Δ/Δ} BCR::ABL1^{p185+} cell lines 12 weeks after initial transformation (n = 4-5 cell lines/genotype, performed in technical duplicates). One representative result out of three independent experiments is depicted. (F) Flow cytometric analysis after PI cell cycle staining of *Ccnc*^{fl/fl} and *Ccnc*^{Δ/Δ} BCR::ABL1^{p185+} cell lines (n=3 stable, independently established cell lines/genotype) in standard medium supplemented with 10% FCS and 24 hours after FCS removal (0% FCS). Experiments were performed in technical duplicates 12-18 weeks after initial transformation. Graphs represent (A, B, D, E, F) mean ± SD. Levels of significance were calculated using (A, B, D) Mann-Whitney U-test, (C) Fisher's exact test or (E) unpaired t-test on log-transformed counts from day 7 post-seeding. *p < 0.05, **p < 0.01, ***p < 0.001, ****p < 0.0001. Abbreviations: BM, bone marrow; IL-7, interleukin-7

Figure 4. Cyclin C deficiency impairs *in vivo* leukemia establishment. (A) Scheme depicting experimental setup of data shown in (B) and (C). 2,500 $Ccnc^{fl/fl}$ or $Ccnc^{\Delta/\Delta}$ BCR::ABL1^{p185+} cells were injected intravenously into NSG mice (n=9-10/genotype, 3 independent cell lines per genotype were injected). (B) Representative pictures of spleens on day 26 post-injection. (C) Representative pictures of blood smears on day 26 post-injection after Hemacolor Rapid staining. Blasts are indicated with turquoise arrows. (D) Scheme depicting experimental setup for data shown in (E) and (F). (E) Intravenous injection of $Ccnc^{fl/fl}$ and $Ccnc^{\Delta/\Delta}$ BCR::ABL1^{p185+} cells into NSG mice (n=9-10/genotype, 3 independent cell lines per genotype were injected, data pooled from two independent experiments). Survival of recipient mice was monitored for up to a maximum of 224-281 days in case of absent disease symptoms. Median survival of mice receiving $Ccnc^{fl/fl}$ injections was 23 days, survival of the only diseased mouse in the $Ccnc^{\Delta/\Delta}$ cohort (highlighted turquoise) was 54 days. Black triangles indicate time points at which mice were eliminated without appearance of disease symptoms. Level of significance was calculated using log-rank (Mantel-Cox) test. (F) Flow cytometric analysis of BM infiltration in mice receiving $Ccnc^{fl/fl}$ and $Ccnc^{\Delta/\Delta}$ BCR::ABL1^{p185+} injections as depicted in (D, E). Graph shows mean \pm SD, level of significance was calculated using Mann-Whitney U-test. ****p < 0.0001. Abbreviations: i.v., intravenously; BM, bone marrow

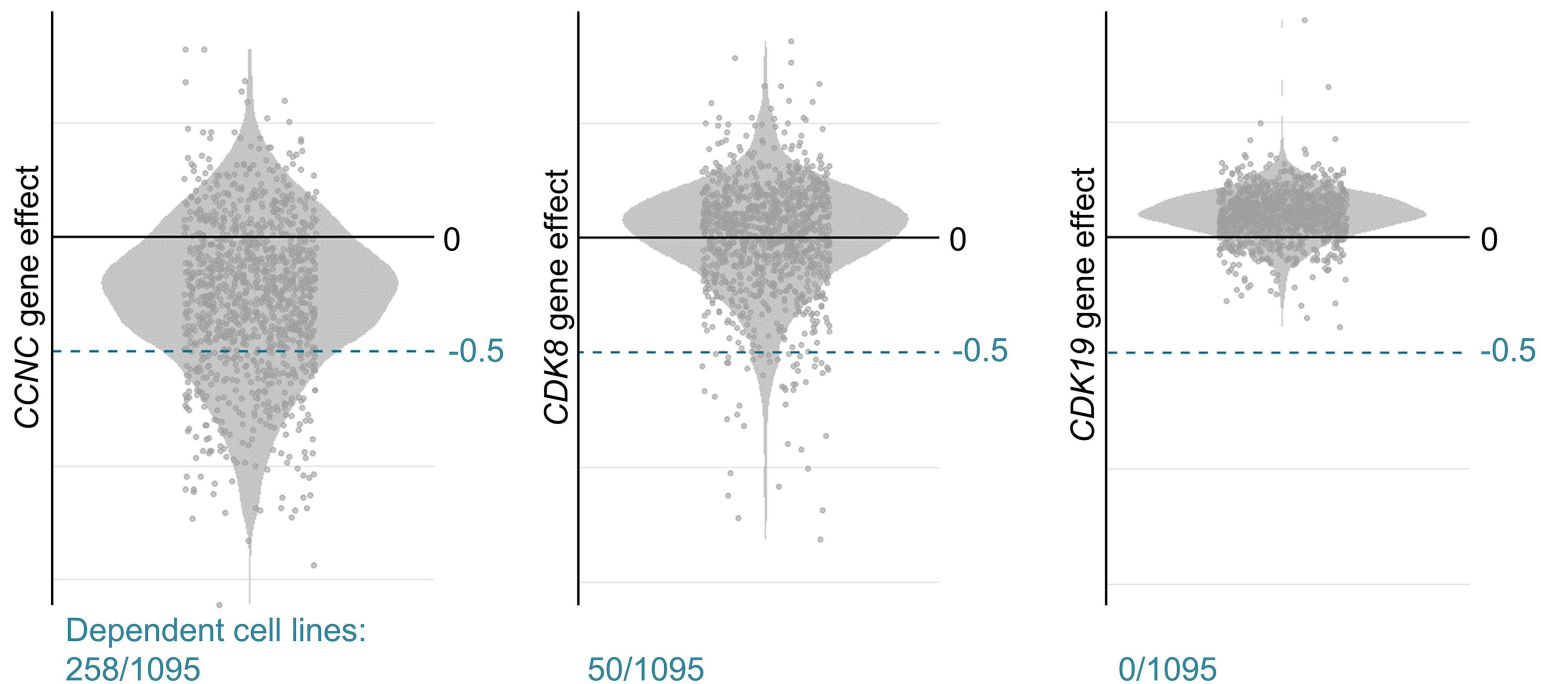
Figure 5. Cyclin C represses p53 responses in transformed cells. (A) Scheme depicting experimental setup for RNA-Seq analyzed in (B) and (C). BM from $Ccnc^{fl/fl}$ and $Ccnc^{fl/fl}$ *VavCre* mice was isolated and infected with retrovirus encoding BCR::ABL1^{p185} to generate stable cell lines (“*in vitro*” samples) which were intravenously (i.v.) injected into NSG mice and retrieved from BM of recipient mice 10 days later (“*ex vivo*” samples). (B) Venn Diagram showing the number of differentially expressed genes (padj < 0.1) in $Ccnc^{\Delta/\Delta}$ vs. $Ccnc^{fl/fl}$ BCR::ABL1^{p185+} cells *in vitro* (blue) and *ex vivo* (orange). Intersecting area shows the overlap between the *in vitro* and *ex vivo* datasets. (C) Significantly upregulated hallmark gene sets (NES>1, FDR<0.2, p<0.05) from GSEA of *ex vivo* derived $Ccnc^{\Delta/\Delta}$ vs. $Ccnc^{fl/fl}$ BCR::ABL1^{p185+} cells which were not significantly enriched in cyclin C deficient BCR::ABL1^{p185+} cell lines *in vitro*. (D) *In vitro* proliferation of $Ccnc^{fl/fl}$ and $Ccnc^{\Delta/\Delta}$ BCR::ABL1^{p185+} cells in standard culture conditions (medium supplemented with 10% FCS,

top), after reducing FCS to 1% (bottom left) and in reduced cell density (bottom right) (n=4-5 cell lines/genotype). (E) Immunoblot analysis of stable $Ccnc^{fl/fl}$ and $Ccnc^{\Delta/\Delta}$ BCR::ABL1^{p185+} cell lines (n=3 per genotype) in standard culture medium (10% FCS) and after reducing FCS to 1% for 24 hours and 96 hours. Levels of cyclin C, cyclin D2, PLK2, NDRG1, GADD45a and 14-3-3σ (*Sfn*) were assessed on three separate immunoblots with the same lysates. HSC70 served as loading control. Abbreviations: RNA-Seq, RNA sequencing; BM, bone marrow; padj, Benjamini-Hochberg adjusted p-value; GSEA, gene set enrichment analysis; EMT, epithelial–mesenchymal transition; ROS, reactive oxygen species; NES, normalized enrichment score; FDR, false discovery rate; FCS, fetal calf serum

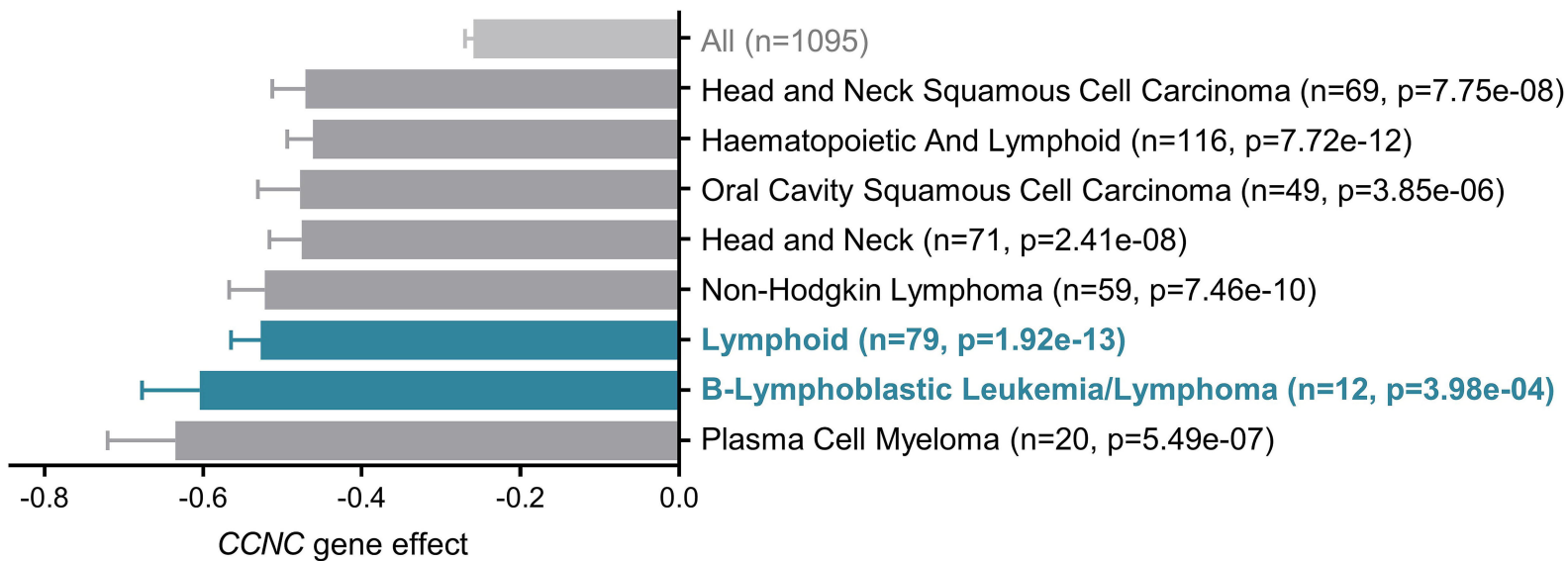
Figure 6. Disruption of functional p53 signaling restores the leukemogenicity of cyclin C deficient BCR::ABL1^{p185+} cells. (A) *In vitro* proliferation of $Ccnc^{fl/fl}$ and $Ccnc^{\Delta/\Delta}$ BCR::ABL1^{p185+} cells six days after direct delivery of a ribonucleoprotein (RNP) complex consisting of Cas9 enzyme and guide RNAs targeting *Gadd45a*, *Sfn* or *Plk2*. A non-targeting control (sgNTC) and mock treated cells (-) served as controls. Growth curves were performed in technical duplicates in standard culture conditions (medium supplemented with 10% FCS, top), with lowered FCS (reduced to 1%, bottom left) or reduced cell density (bottom right). Graphs show mean ± SD. Levels of significance were determined by one-way ANOVA followed by Dunnett's test comparing log-transformed counts from day 6 post-seeding with sgNTC as control group for $Ccnc^{fl/fl}$ and $Ccnc^{\Delta/\Delta}$ BCR::ABL1^{p185+} cells, respectively. (B) Immunoblot analysis showing levels of cyclin C and p53 in spleen infiltrating BCR::ABL1^{p185+} cells of diseased mice from experiment depicted in **Figure 4E**. HSC70 served as loading control. (C) Kaplan–Meier plot of NSG mice after intravenous injection of $Ccnc^{fl/fl}$ and $Ccnc^{\Delta/\Delta}$ BCR::ABL1^{p185+} cells carrying spontaneous mutations in the DNA binding domain of p53 (p53^{mut}) (n = 4 per genotype, median survival 16 vs. 18 days). (D) Stable $Ccnc^{fl/fl}$ and $Ccnc^{\Delta/\Delta}$ BCR::ABL1^{p185+} cell lines were infected with retrovirus encoding dominant negative p53 (dn p53), intravenously injected into NSG mice and survival was monitored (2 independent cell lines per genotype were used, n=5 mice were injected with $Ccnc^{fl/fl}$ + dn p53 and n=5 received $Ccnc^{\Delta/\Delta}$ + dn p53 BCR::ABL1^{p185+} cells, median survival 20 vs. 22 days). Levels of significance were determined using (C, D) log-rank (Mantel–Cox) test. *p < 0.05, **p < 0.01, ***p < 0.001. Abbreviations: FCS, fetal calf serum

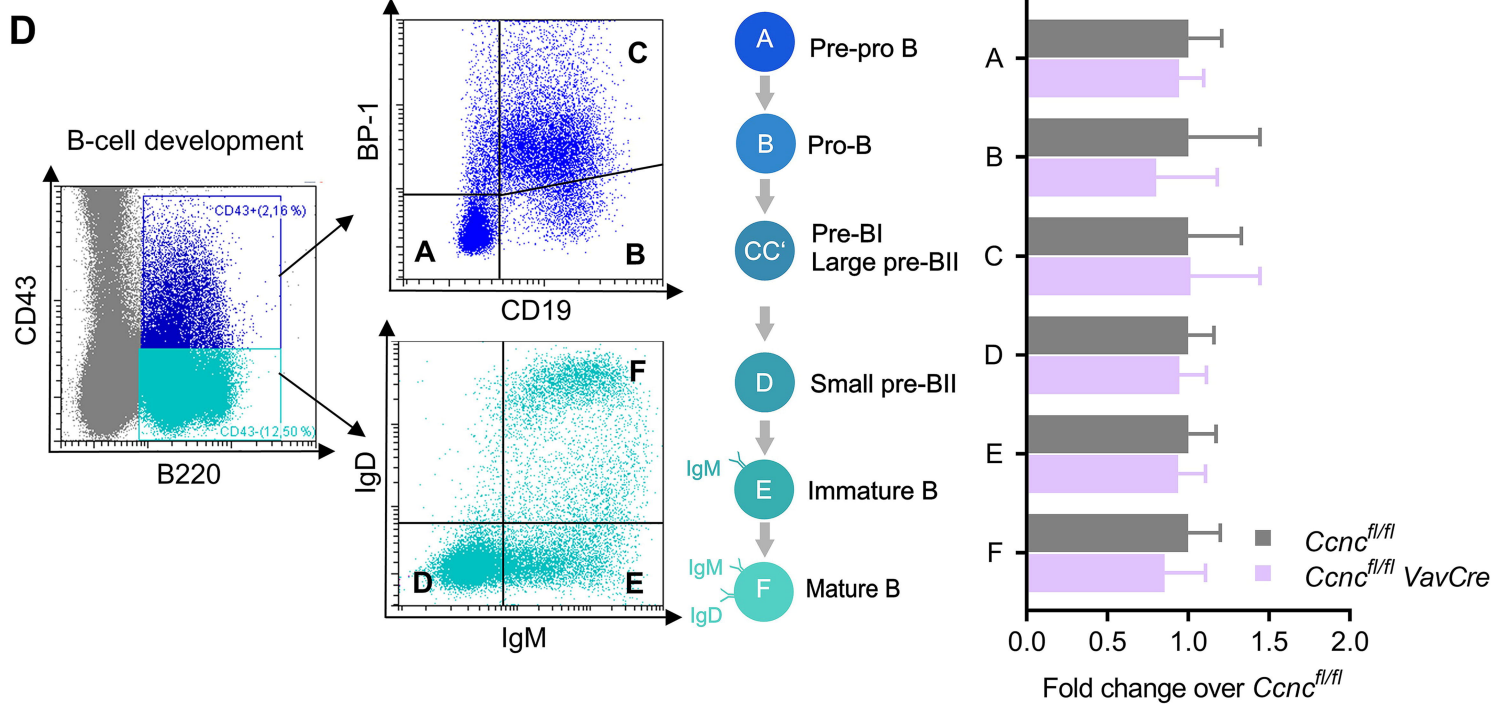
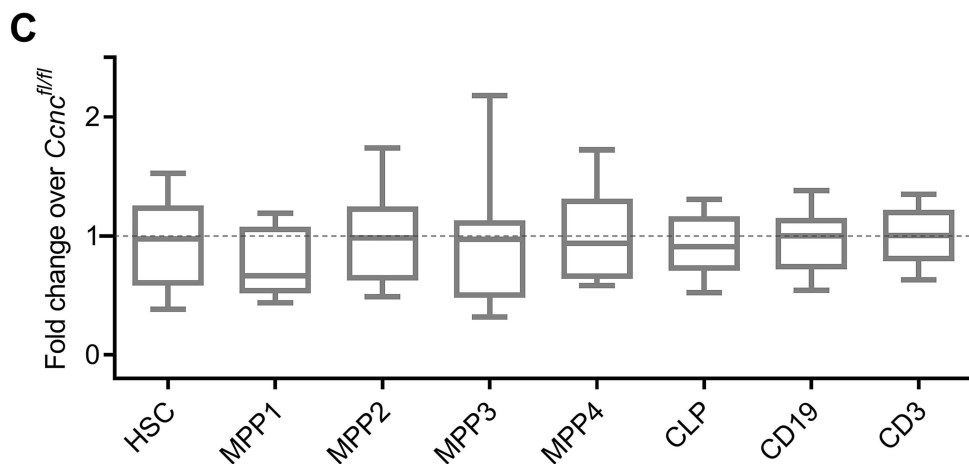
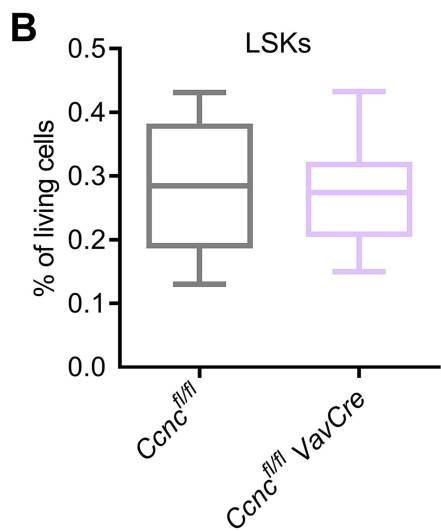
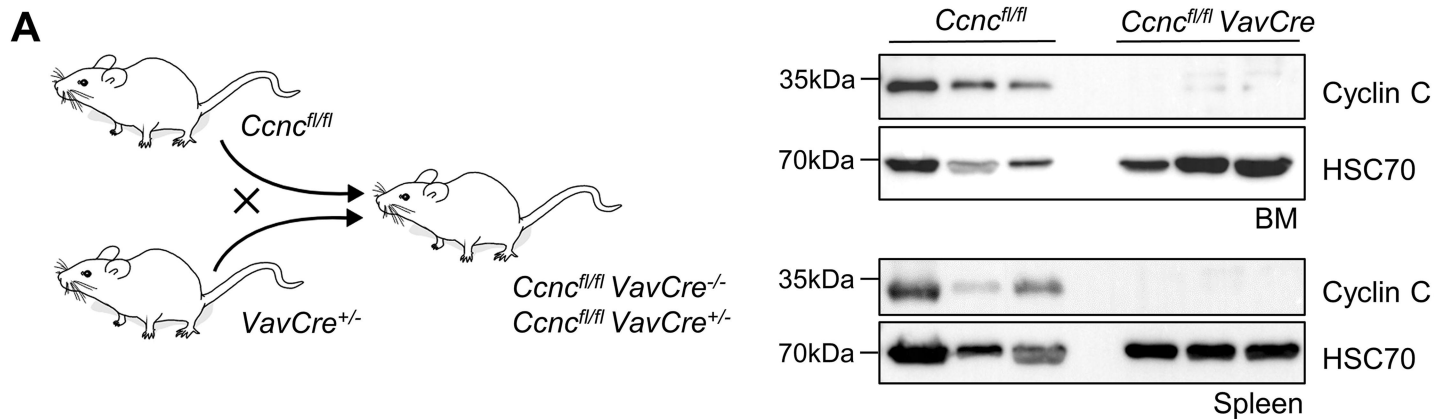
Figure 7. Cyclin C as a potential new target for B-ALL treatment. (A) Gene expression profile of *CCNC* in control (BM mononuclear cells, n=56) versus primary B-cell precursor acute lymphoblastic leukemia (BCP-ALL) samples (n=362), presented as violin plot. (Sample size per subtype: *BCR::ABL1*: n = 97; *BCR::ABL1*-like: n = 51; *ETV6::RUNX1*: n = 6; *KMT2A* rear: n = 56; *ZNF384* rear: n = 20; low hypodiploid: n = 45; high hyperdiploid: n = 17; near haploid: n = 2; *TCF3::PBX1*: n = 6; *DUX4* rear: n = 22; *PAX5* P80R: n = 14; *PAX5*alt: n = 10; *BCL2/MYC*: n = 4; *CDX2/UBTF*: n = 7; *NUTM1* rear: n = 2; *ZEB2/CEBP*: n = 3). (B) Analysis of 12 human B-lymphoblastic leukemia/lymphoma cell lines showing p53 status and dependency probabilities for *CCNC* from a genome-wide CRISPR/Cas9 knock-out screen (DepMap Public 23Q2+Score, Chronos). Cell lines with dependency probabilities greater than 0.5 are considered dependent. (C) Immunoblot showing cyclin C levels in bulk cell culture after CRISPR/Cas9 mediated targeting of cyclin C in NALM-6 cells. Three different guide RNAs targeting cyclin C (sgCCNC) were used, guide RNA targeting *HPRT1* served as control (ctrl). HSC70 was used as loading control. (D) Bulk cell lines depicted in (E) were single cell sorted using a BD FACSAria III cell sorter and outgrowth of single cell clones was monitored. One representative result is shown, a similar result was obtained using limiting dilution to generate monoclonal cell lines. (E) Probability of event-free survival (EFS) in pediatric BCP-ALL patients with high versus low *CCNC* expression. The high/low *CCNC* cut-off was based on median expression among BCP-ALL samples in cohort. Death in induction, death, relapse, nonresponse and secondary malignancy were counted as events for EFS. (F) Proportion of pediatric BCP-ALL patients who reached remission after induction treatment, but for which an event (relapse/death) was reported prior to 36 months. Error bars represent 95% confidence interval calculated using the adjusted Wald method. Levels of significance were determined using (E) log-rank (Mantel–Cox) test and (F) Fisher’s exact test. ****p<0.0001. Abbreviations: BM, bone marrow; EFS, event-free survival

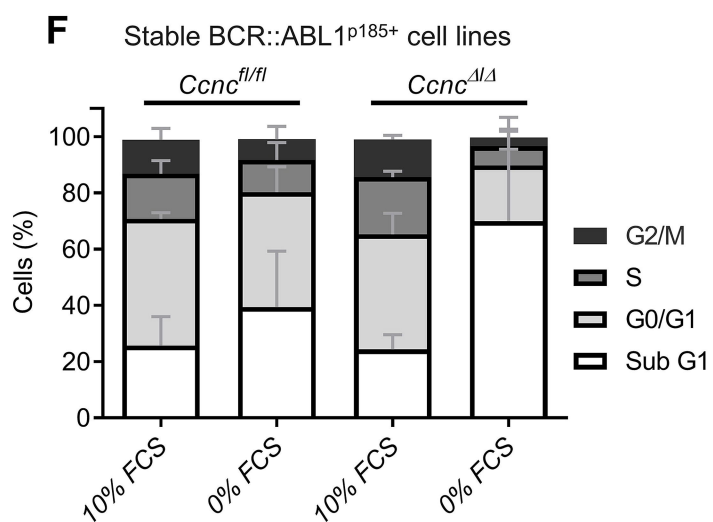
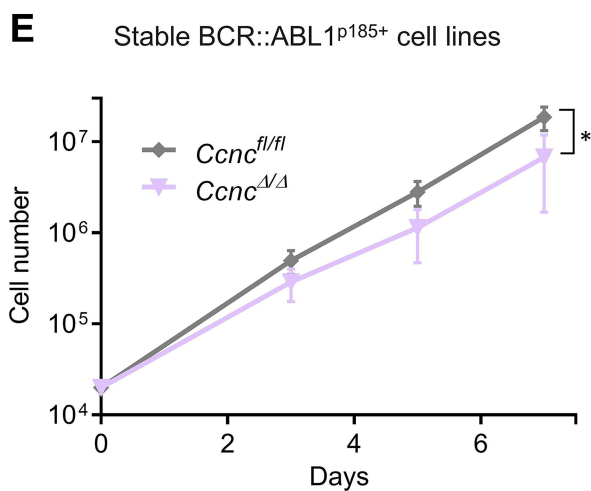
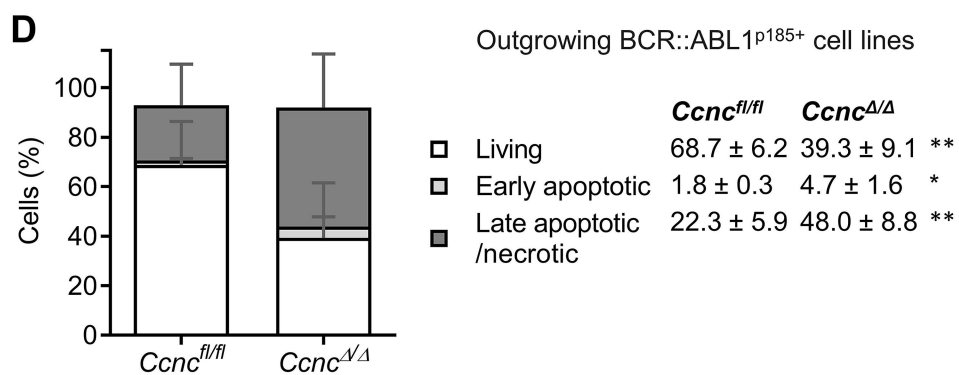
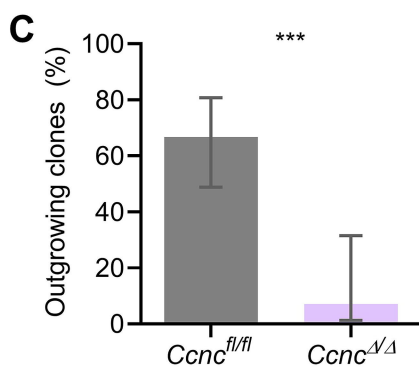
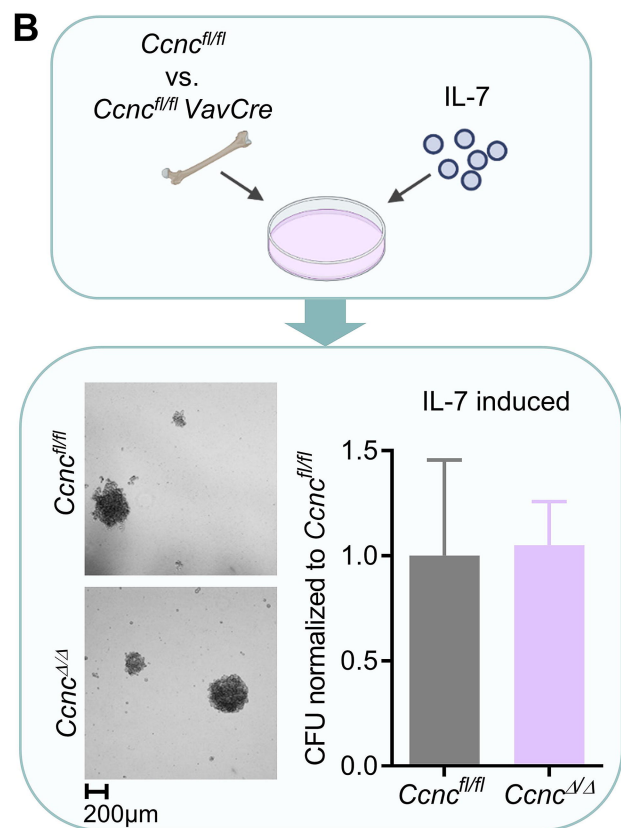
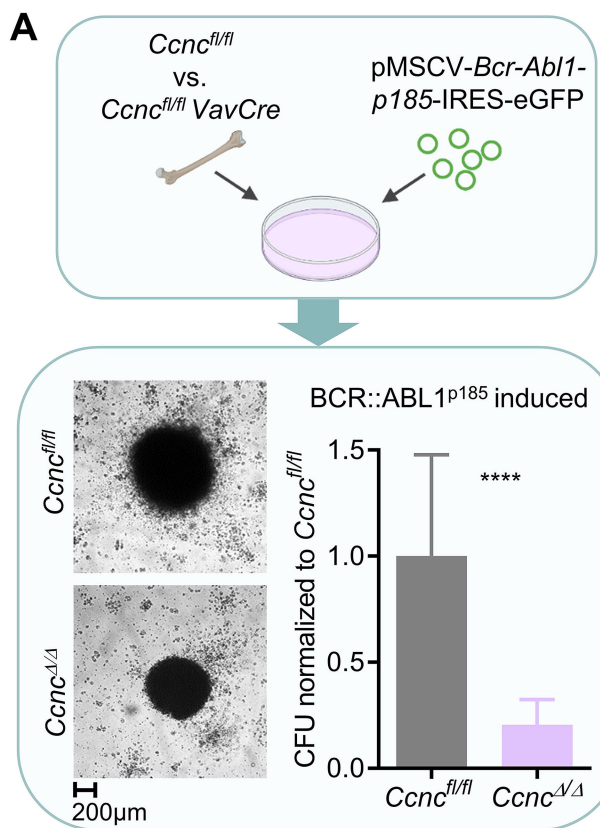
A Cell lines/CRISPR knockout screen
Broad Institute Cancer Dependency Map

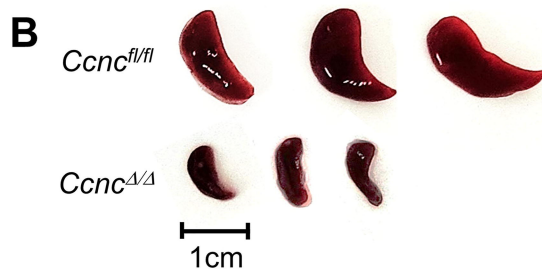
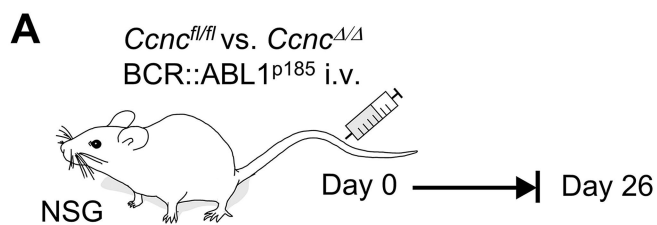


B

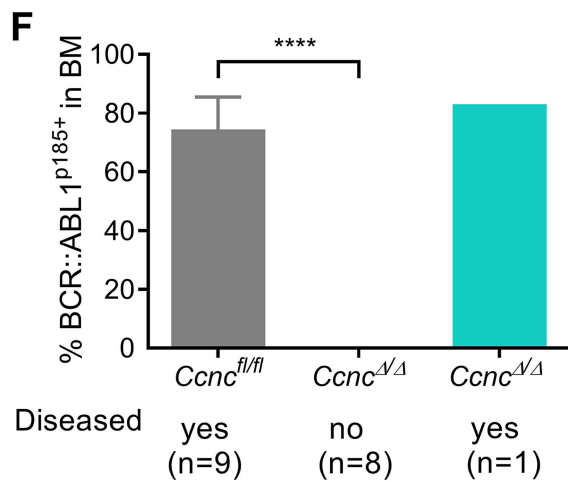
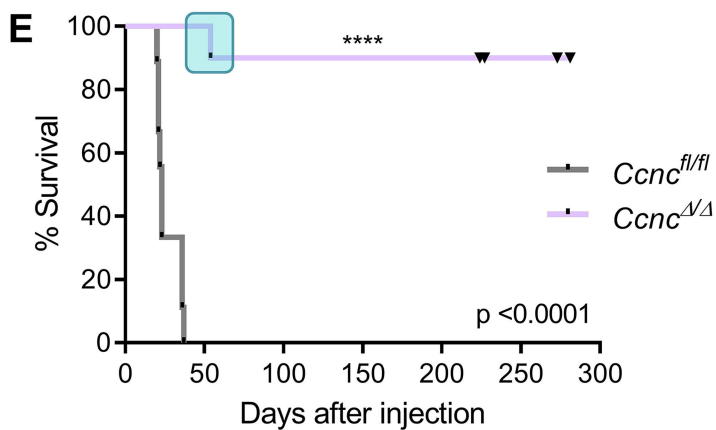
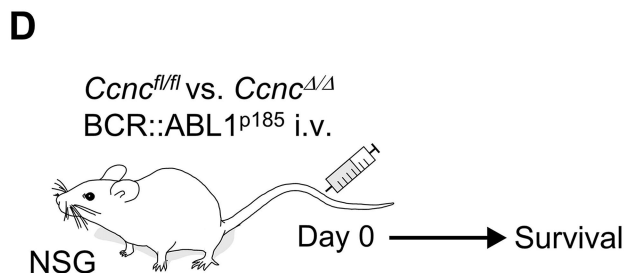
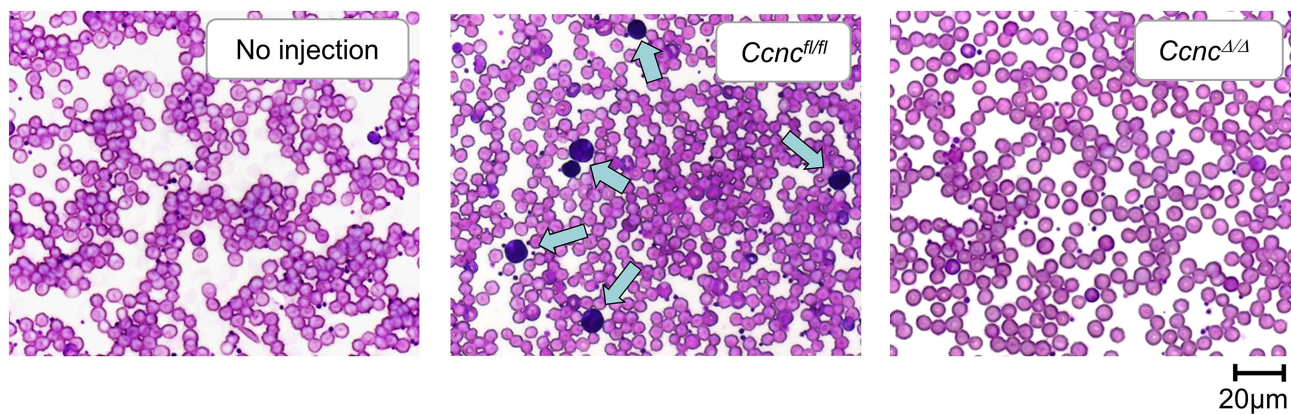


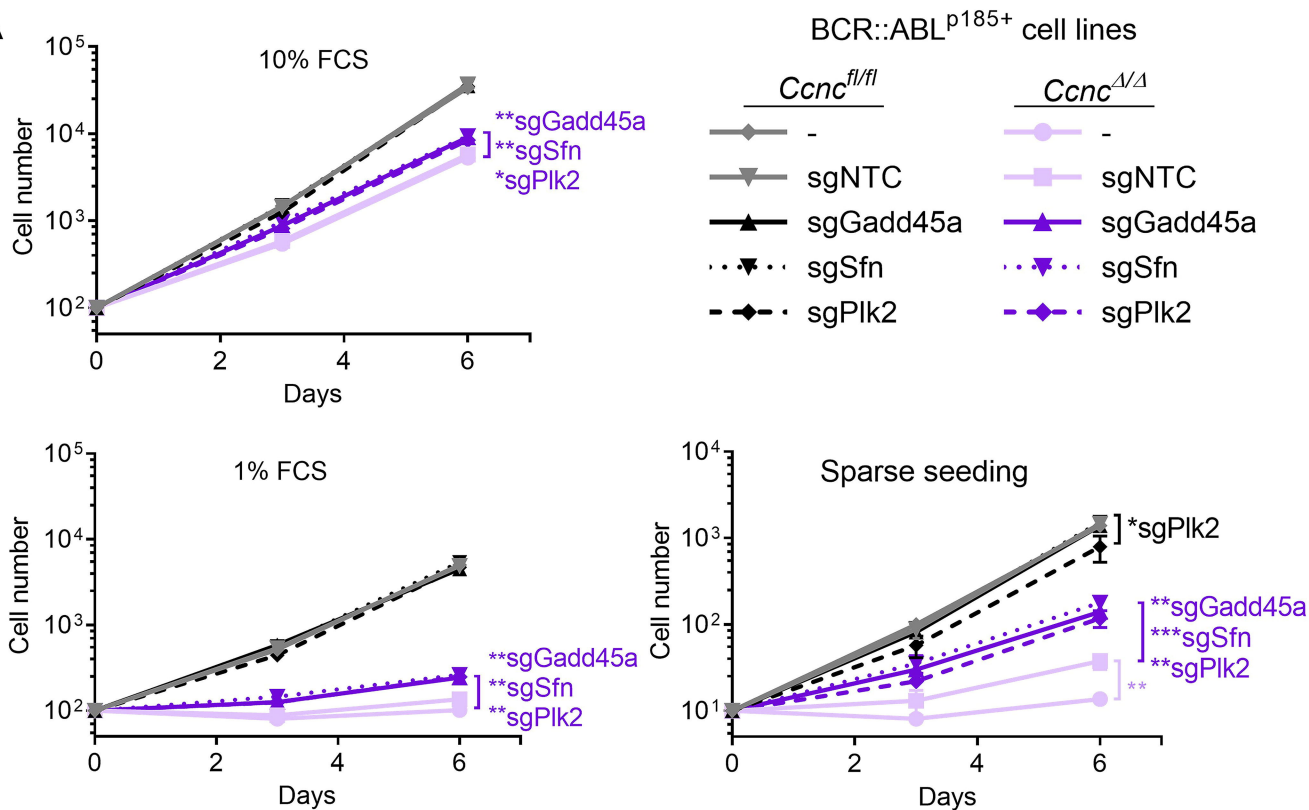
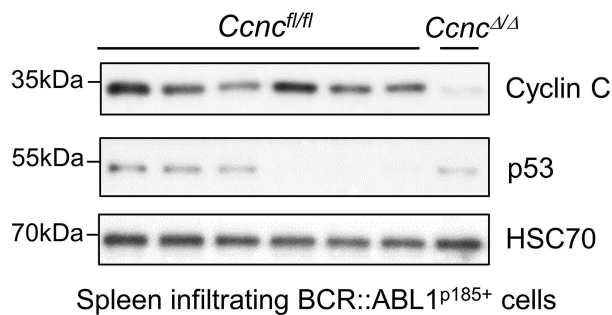
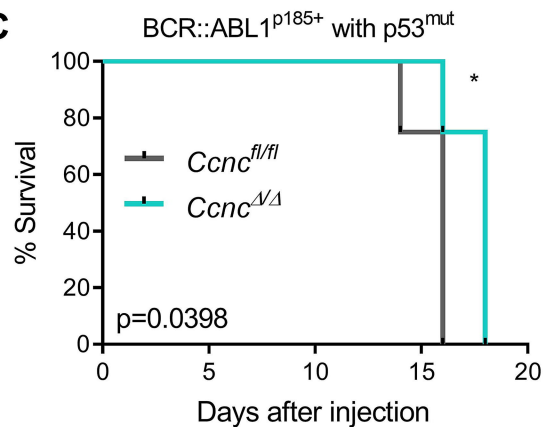
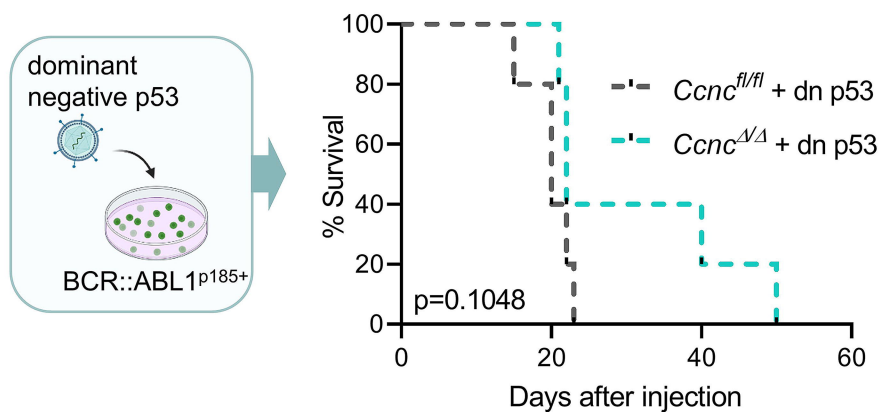


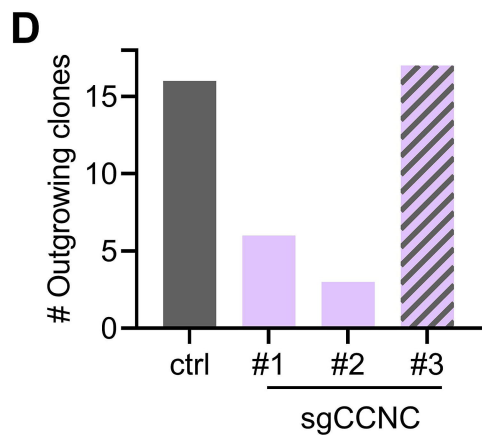
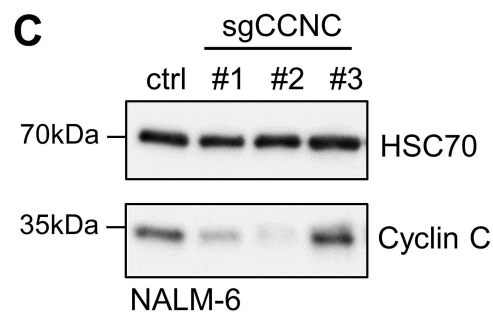
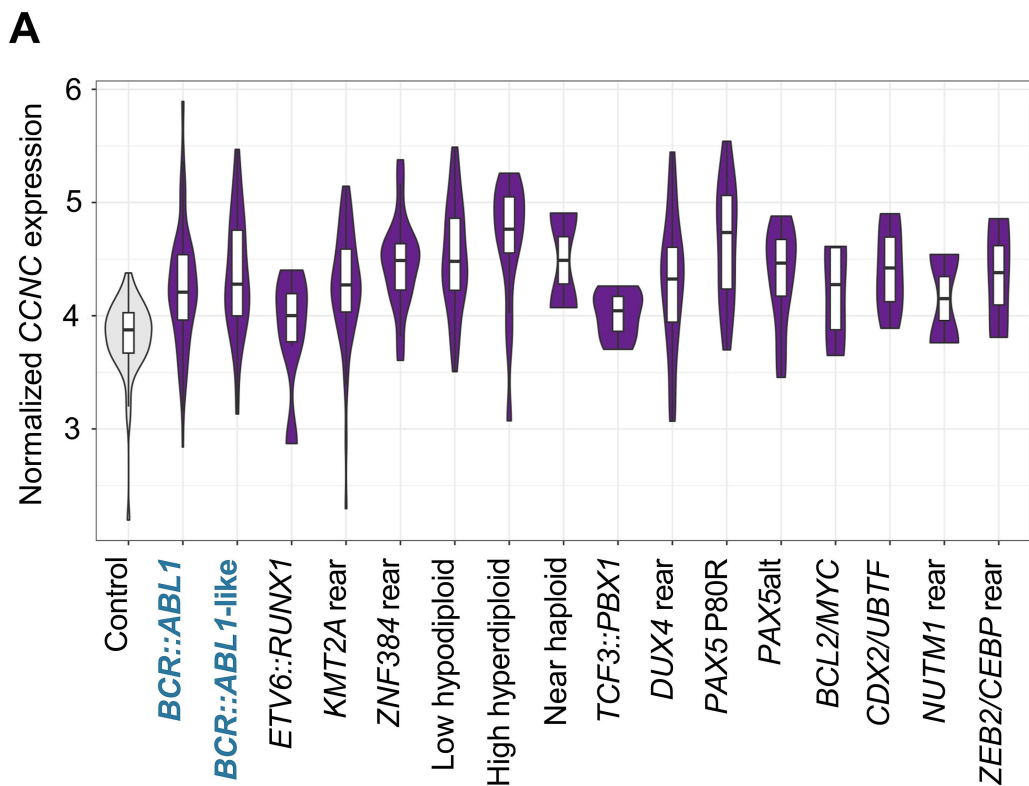




C Blood

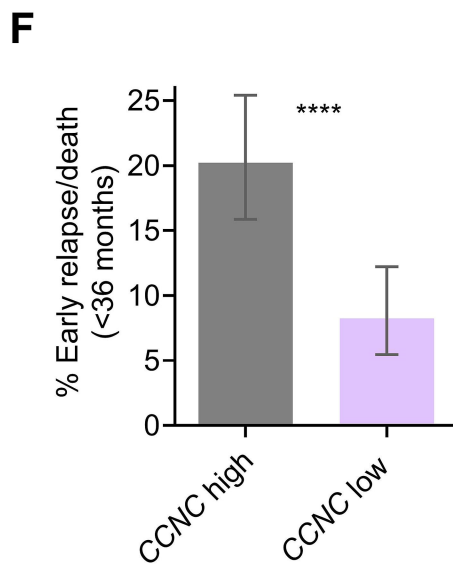
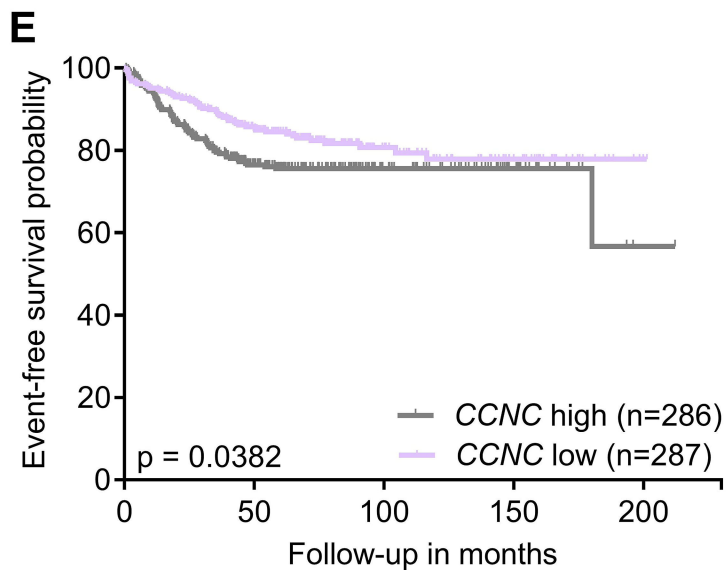


A**B****C****D**



B

Cell line	HG-3	697	JM1	RCH-ACV	NALM-6	P30/OHK	TANOUE	NALM-16	Reh	SEM	SEMK2	HB1119
Probability of dependency	0.41	0.84	0.95	0.79	0.85	0.83	0.30	0.13	0.27	0.47	0.87	0.99
CCNC dependency		x	x	x	x	x					x	x
<i>TP53</i> wildtype	x	x	x	x	x	x						



Supplementary Information

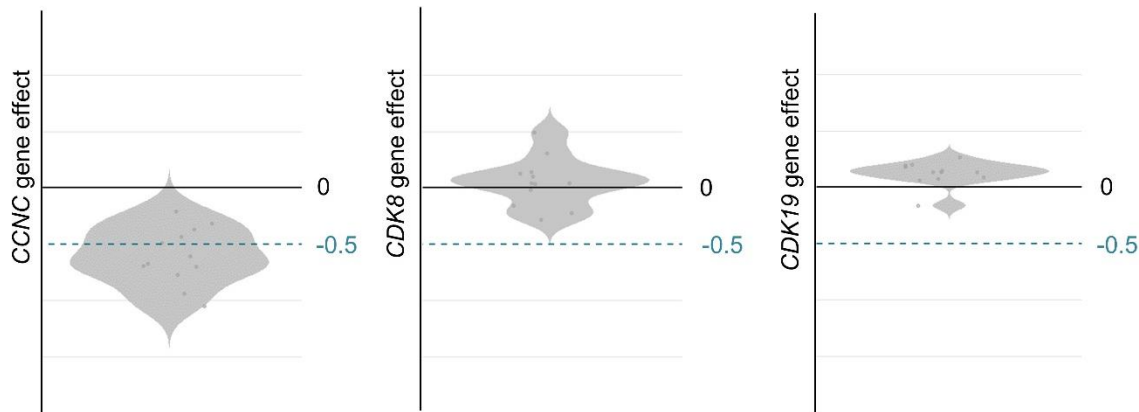
Cyclin C promotes development and progression of B-cell acute lymphoblastic leukemia by counteracting p53-mediated stress responses

This file includes the Supplementary Figures and Figure Legends, Supplementary Materials and Methods, Supplementary Tables and Supplementary References

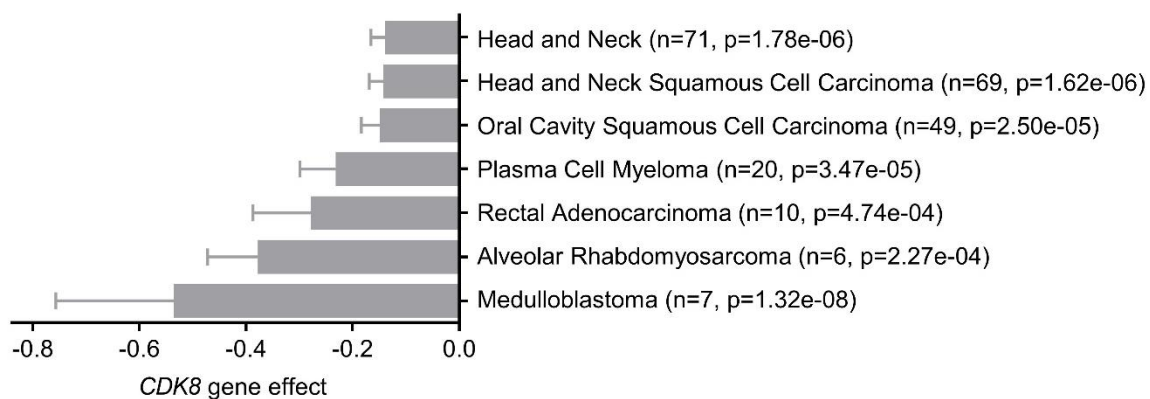
Supplementary Figures

Supplementary Figure 1

A B-lymphoblastic leukemia/lymphoma cell lines, CRISPR knockout screen Broad Institute Cancer Dependency Map

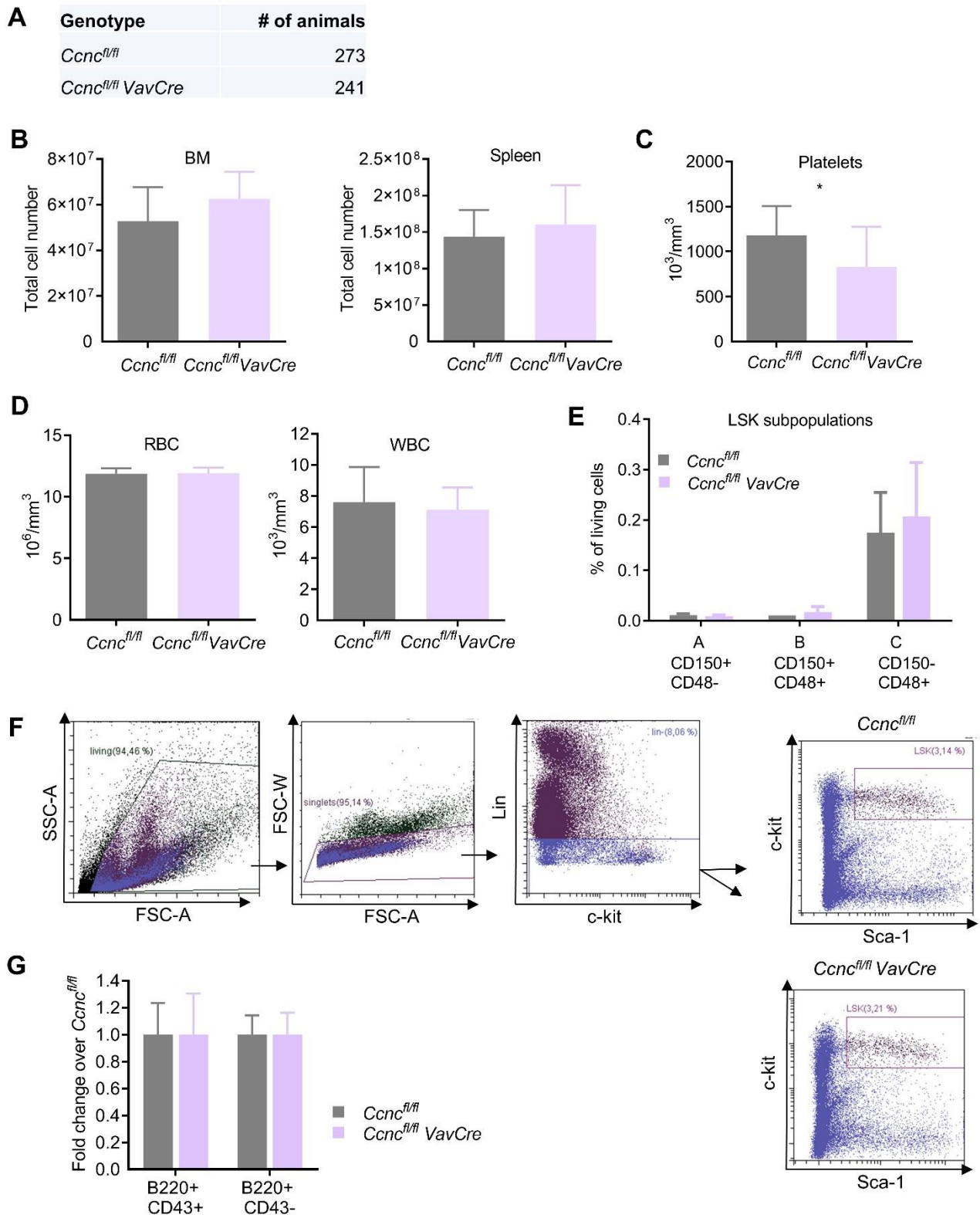


B



Supplementary Figure 1. (A) CRISPR dependencies for *CCNC*, *CDK8* and *CDK19* as in **Figure 1A**, filtered for cell lines annotated as B-lymphoblastic leukemia/lymphoma (n=12). Dependency score obtained from the Broad Institute Cancer Dependency Map (DepMap Public 23Q2+Score, Chronos). **(B)** Enrichment plot for the top 7 significantly ($p < 0.0005$, t-test) enriched lineages based on the Broad Institute Cancer Dependency Map (Depmap) CRISPR dependencies for *CDK8*. The number of cell lines included in each lineage subset is denoted in parentheses and ranking was done based on effect size.

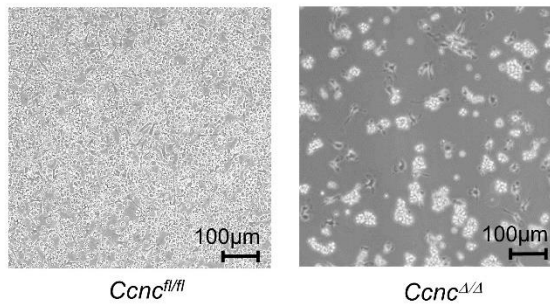
Supplementary Figure 2



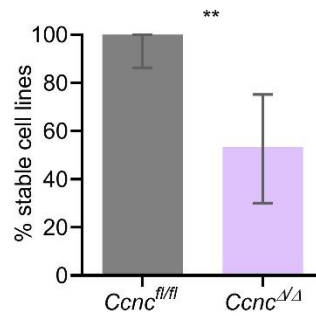
Supplementary Figure 2. (A) Table indicating the genotype of offspring from breedings between $Ccnc^{fl/fl} VavCre^{-/-}$ ($Ccnc^{fl/fl}$) and $Ccnc^{fl/fl} VavCre^{+/-}$ ($Ccnc^{fl/fl} VavCre$) mice (n = 514 offspring, p = 0.158). (B) Total counts of living BM (femur and tibia of both hind legs) and splenic cells of $Ccnc^{fl/fl}$ and $Ccnc^{fl/fl} VavCre$ mice (n = 10-12/genotype). (C) Platelet count of $Ccnc^{fl/fl}$ and $Ccnc^{fl/fl} VavCre$ mice (n=9-14/genotype), pooled from two independent experiments. (D) Analysis of red blood cell count (RBC) and white blood cell count (WBC) of $Ccnc^{fl/fl}$ and $Ccnc^{fl/fl} VavCre$ mice (n=9-14/genotype), pooled from two independent experiments. (E) Frequencies of LSK fractions A,B and C in bone marrow of $Ccnc^{fl/fl}$ and $Ccnc^{fl/fl} VavCre$ mice based on expression of CD48 and CD150 (n=10-12/genotype). (F) Representative FACS plots for LSK cells in bone marrow of $Ccnc^{fl/fl}$ and $Ccnc^{fl/fl} VavCre$ mice. (G) Relative fold change of B220+CD43 \pm subpopulations in BM of $Ccnc^{fl/fl} VavCre$ (n = 10) normalized to the mean value from $Ccnc^{fl/fl}$ mice (n = 12). Bar graphs show mean \pm SD. Levels of significance were calculated using (A) chi-square test, (B) unpaired t-test or (C, D, E, G) Mann-Whitney U-test. *p < 0.05. Abbreviations: BM, bone marrow; LSK, Lin $^-$ Sca-1 $^+$ c-kit $^+$

Supplementary Figure 3

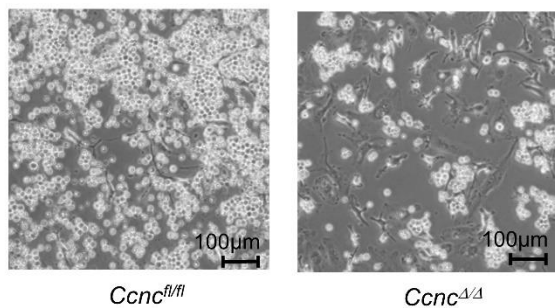
A BCR::ABL1^{p185+} 12 days after transformation



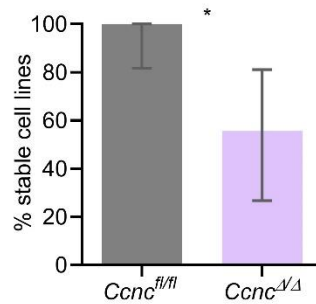
B



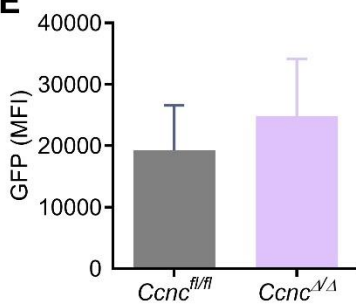
C v-ABL1^{p160} 14 days after transformation



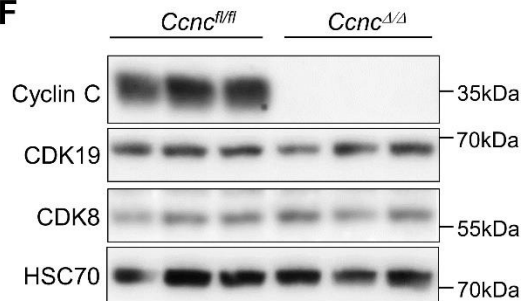
D



E



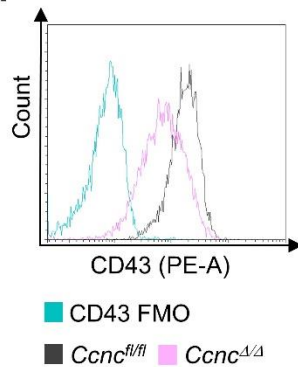
F



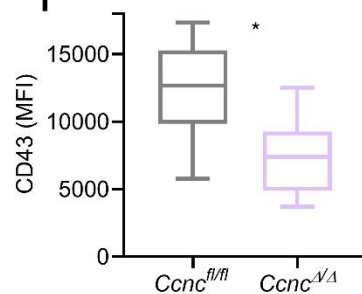
G

	IgM- IgD- (%)	B220+ CD19+ (%)
<i>Ccnc</i> ^{fl/fl}	97.8 ± 2.4	98.8 ± 1.5
<i>Ccnc</i> ^{ΔΔ}	95.8 ± 5.2	98.9 ± 0.8

H

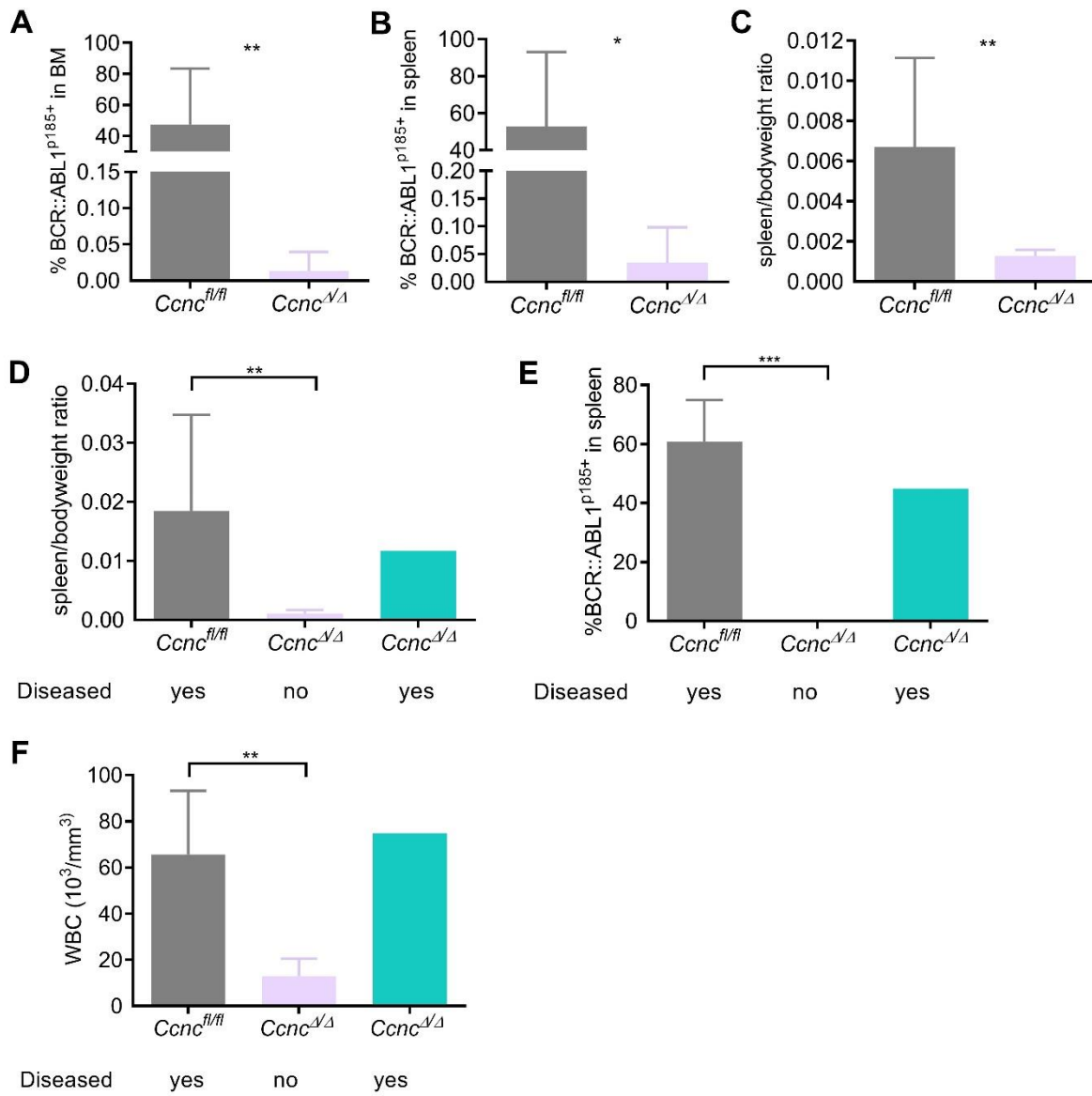


I



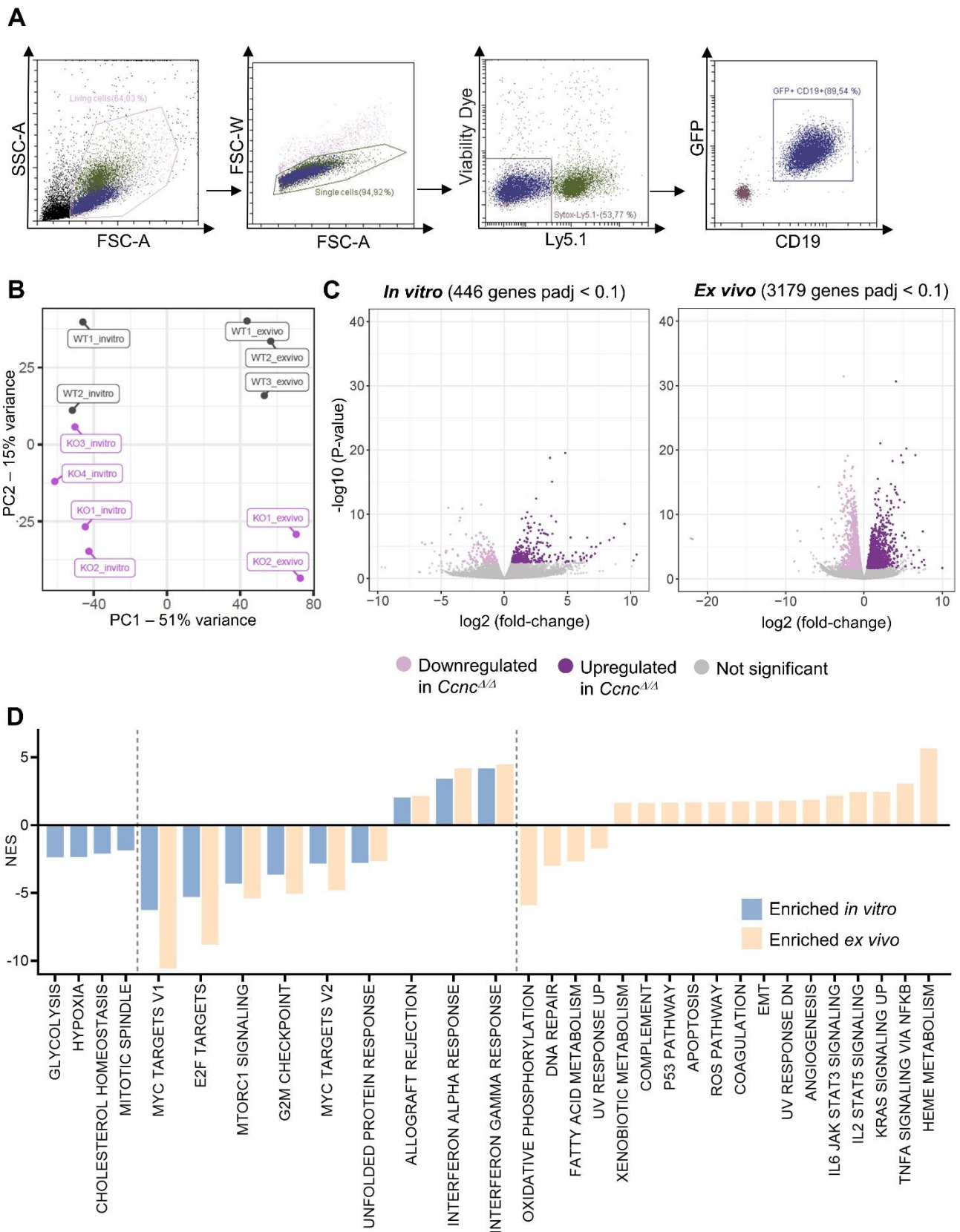
Supplementary Figure 3. (A-D) BM from *Ccnc*^{f/f} and *Ccnc*^{f/f} *VavCre* mice (n=9/genotype) was transformed with either the *BCR::ABL1*^{p185+} or the *v-ABL1*^{p160+} oncogene. Microscopic photographs show representative pictures of cells (A) 12 or (C) 14 days after transformation. Outgrowth of stable cell lines was monitored and outcome summarized in (B) and (D). Error bars represent confidence intervals calculated using the Wilson Score interval (95% confidence level). **(E)** Flow cytometric analysis of GFP expression in stable cell lines established from BM of *Ccnc*^{f/f} and *Ccnc*^{f/f} *VavCre* mice infected with retrovirus encoding pMSCV-*BCR::ABL1-p185-IRES-eGFP* (n=6-10/genotype). Error bars represent mean ± SD. **(F)** Immunoblotting for levels of cyclin C, CDK8 and CDK19 in stable *BCR::ABL1*^{p185+} cell lines. HSC70 served as loading control. **(G)** Table indicating frequencies of *Ccnc*^{f/f} and *Ccnc*^{Δ/Δ} *BCR::ABL1*^{p185+} cells staining negative for IgM and IgD and double positive for B220 and CD19 (n=7-11/genotype). **(H)** Representative histogram showing CD43 expression of living *Ccnc*^{f/f} and *Ccnc*^{Δ/Δ} *BCR::ABL1*^{p185+} cells and **(I)** quantitative analysis (n=7-11/genotype). Center value represents median, the box 25th to 75th percentiles, and whiskers min to max. Levels of significance were calculated using (B,D) Fisher's exact test, (E, G, I) Mann-Whitney U-test. *p < 0.05, **p < 0.01. Abbreviations: BM, bone marrow; MFI, median fluorescence intensity

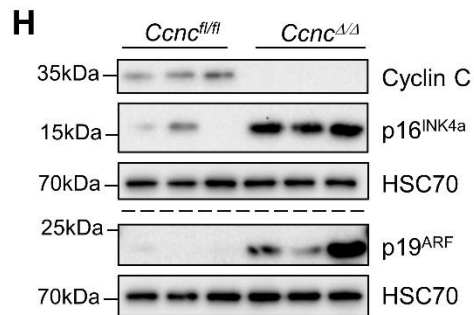
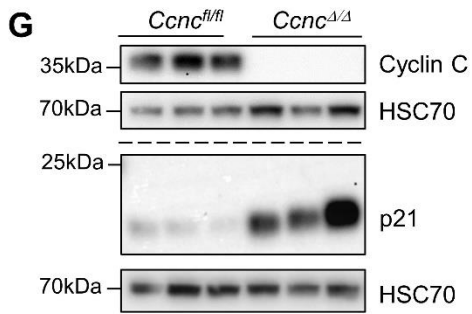
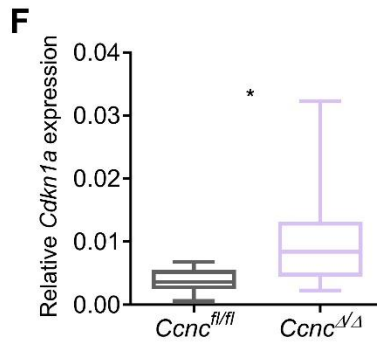
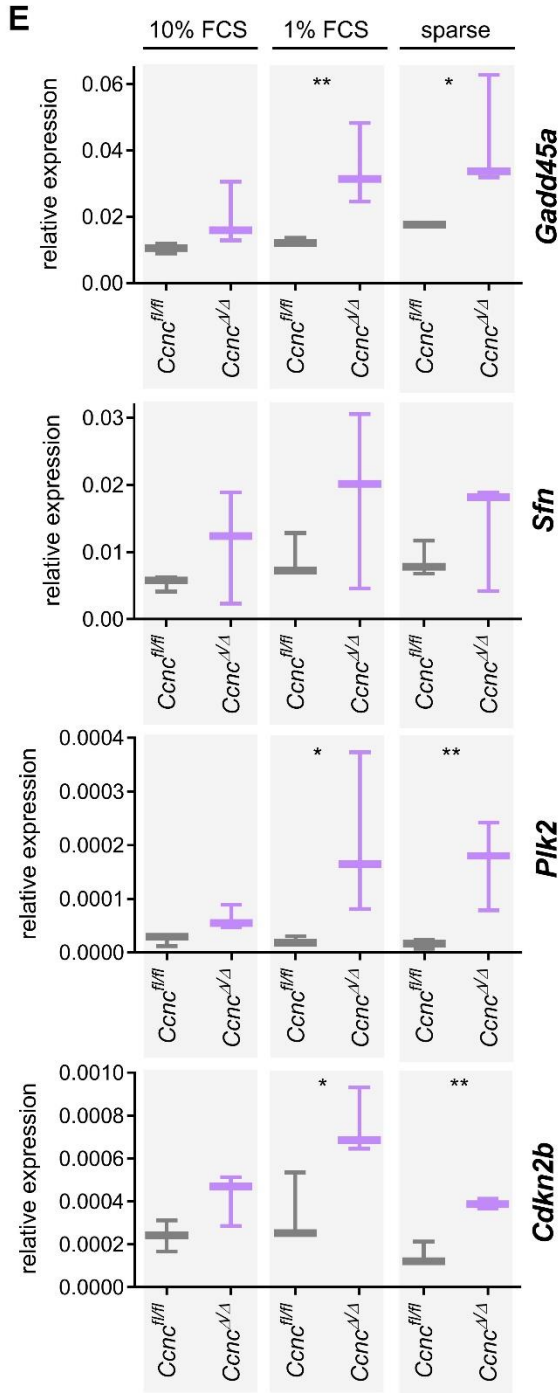
Supplementary Figure 4



Supplementary Figure 4. (A-C) $Ccnc^{fl/fl}$ or $Ccnc^{\Delta/\Delta}$ BCR::ABL1^{p185+} cells were intravenously injected into NSG mice and recipient mice were analyzed for disease progression after 26 days (n=9-10 per genotype). (A) Infiltration of BCR::ABL1^{p185+} cells in BM of recipient mice. (B) Splenic infiltration of BCR::ABL1^{p185+} cells 26 days after injection. (C) Analysis of spleen weights normalized to body weight at day 26 post-injection. (D-F) $Ccnc^{fl/fl}$ or $Ccnc^{\Delta/\Delta}$ BCR::ABL1^{p185+} cells were intravenously injected into NSG mice (n=9-10/genotype) and survival was monitored for up to a maximum of 224-281 days in case of absent disease development. Bar graphs show analysis of diseased mice from $Ccnc^{fl/fl}$ cohort compared to mice receiving $Ccnc^{\Delta/\Delta}$ BCR::ABL1^{p185+} cell injections of which only one showed disease symptoms. (D) Spleen weights normalized to body weight of recipient mice ($Ccnc^{fl/fl}$ (n=9), healthy $Ccnc^{\Delta/\Delta}$ (n=9), diseased $Ccnc^{\Delta/\Delta}$ (n=1)). (E) Frequencies of BCR::ABL1^{p185+} cells in spleens of recipient mice ($Ccnc^{fl/fl}$ (n=9), healthy $Ccnc^{\Delta/\Delta}$ (n=5), diseased $Ccnc^{\Delta/\Delta}$ (n=1)). (F) White blood cell count (WBC) in mice receiving $Ccnc^{fl/fl}$ BCR::ABL1^{p185+} injections compared with $Ccnc^{\Delta/\Delta}$ cohort ($Ccnc^{fl/fl}$ (n=5), healthy $Ccnc^{\Delta/\Delta}$ (n=4), diseased $Ccnc^{\Delta/\Delta}$ (n=1)). Graphs show mean \pm SD. Mann-Whitney U-test (A, B, E) or unpaired t-test (C, D, F) were used to calculate levels of significance. *p < 0.05, **p < 0.01, ***p < 0.001. Abbreviations: BM, bone marrow

Supplementary Figure 5

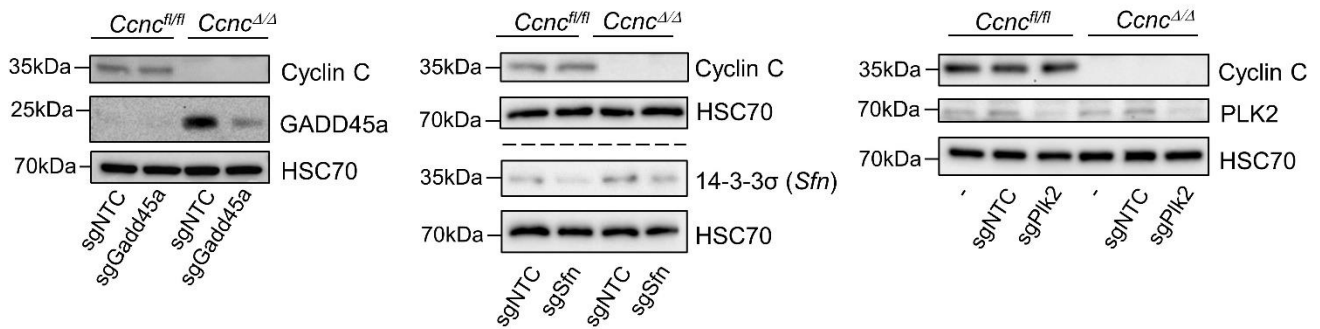




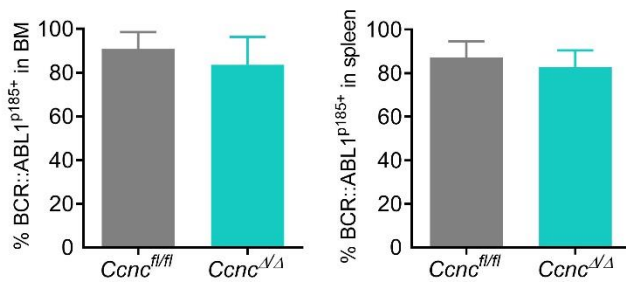
Supplementary Figure 5. (A) Representative flow cytometric plots showing the gating strategy for retrieval of BCR::ABL1^{p185+} cells from BM of inoculated NSG mice. Ten days after intravenous injection of NSG mice with BCR::ABL1^{p185+} cells, living Ly5.1⁻CD19⁺GFP⁺ cells were sorted and used for subsequent RNA-Seq analyses (*ex vivo* samples). (B) Principal Component Analysis (PCA) of stable *Ccnc*^{fl/fl} (WT) and *Ccnc*^{Δ/Δ} (KO) BCR::ABL1^{p185+} cell lines before (*in vitro*) and after injection into NSG mice (*ex vivo*, retrieved from BM 10 days post-injection). (C) Volcano plots of differentially expressed genes (padj <0.1) in *Ccnc*^{Δ/Δ} BCR::ABL1^{p185+} vs. *Ccnc*^{fl/fl} BCR::ABL1^{p185+} cells before injection into NSG mice (*in vitro*, left) and after retrieval from BM of recipient mice (*ex vivo*, right). (D) GSEA results showing significantly (|NES| >1, FDR <0.2, p <0.05) enriched hallmark gene sets in *Ccnc*^{Δ/Δ} BCR::ABL1^{p185+} vs. *Ccnc*^{fl/fl} BCR::ABL1^{p185+} cells. Gene sets only enriched *in vitro* are shown on the left, commonly enriched gene sets in the middle, and gene sets uniquely enriched in *ex vivo* samples are depicted on the right. (E) Expression of genes that contributed to core enrichment of the hallmark p53 pathway gene set in *ex vivo* derived *Ccnc*^{Δ/Δ} BCR::ABL1^{p185+} cells were evaluated via RT-qPCR of RNA extracted from *in vitro* cultured *Ccnc*^{fl/fl} and *Ccnc*^{Δ/Δ} BCR::ABL1^{p185+} cells in different conditions (cells cultured in standard medium supplemented with 10% FCS (left panel), with reduced FCS (1%, middle panel) and with reduced cell density (right panel)). Expression levels were normalized to *Actb*. Experiment was performed in technical duplicates of n=3 independent cell lines/genotype. Center value represents median, the box 25th to 75th percentiles, and whiskers min to max. (F) Expression of *Cdkn1a* relative to *Rplp0* of *Ccnc*^{fl/fl} (n=10) and *Ccnc*^{Δ/Δ} BCR::ABL1^{p185+} (n=8) cell lines from two independent qRT-PCR experiments performed in technical duplicates. Center values represent median of biological replicates, the box 25th to 75th percentiles, and whiskers min to max. (G) Analysis of cyclin C and p21 protein levels on two separate immunoblots showing the same *Ccnc*^{fl/fl} versus *Ccnc*^{Δ/Δ} BCR::ABL1^{p185} cell line lysates (n=3 independent cell lines per genotype). HSC70 served as loading control. (H) Immunoblot analysis of p16^{INK4a} and p19^{ARF} levels in *Ccnc*^{fl/fl} versus *Ccnc*^{Δ/Δ} BCR::ABL1^{p185} cells (n=3 biological replicates per genotype). Analysis was performed on two separate immunoblots with the same lysates, HSC70 was used as loading control. Levels of significance (E,F) were calculated using unpaired t-test on ΔCt values. *p < 0.05, **p < 0.01. Abbreviations: RNA-Seq, RNA sequencing; BM, bone marrow; PC, principal component; padj, Benjamini-Hochberg adjusted p-value; GSEA, gene set enrichment analysis; EMT, epithelial–mesenchymal transition; ROS, reactive oxygen species; NES, normalized enrichment score; FDR, false discovery rate; RT-qPCR, real-time quantitative PCR; FCS, fetal calf serum

Supplementary Figure 6

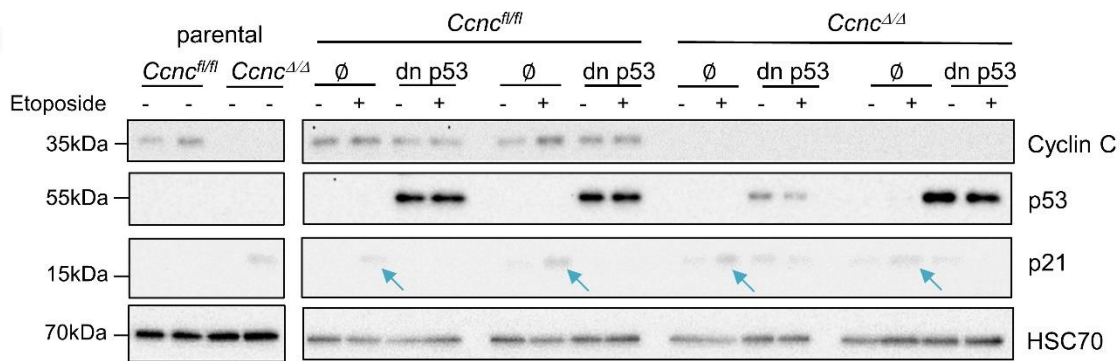
A



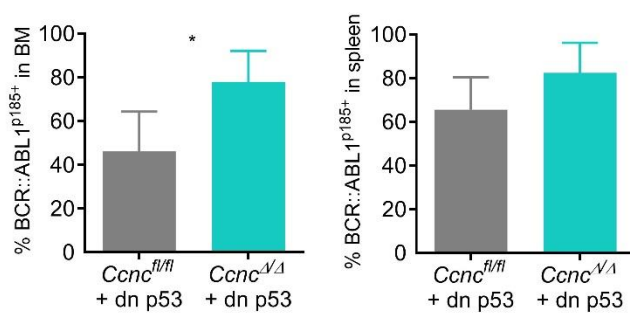
B



C

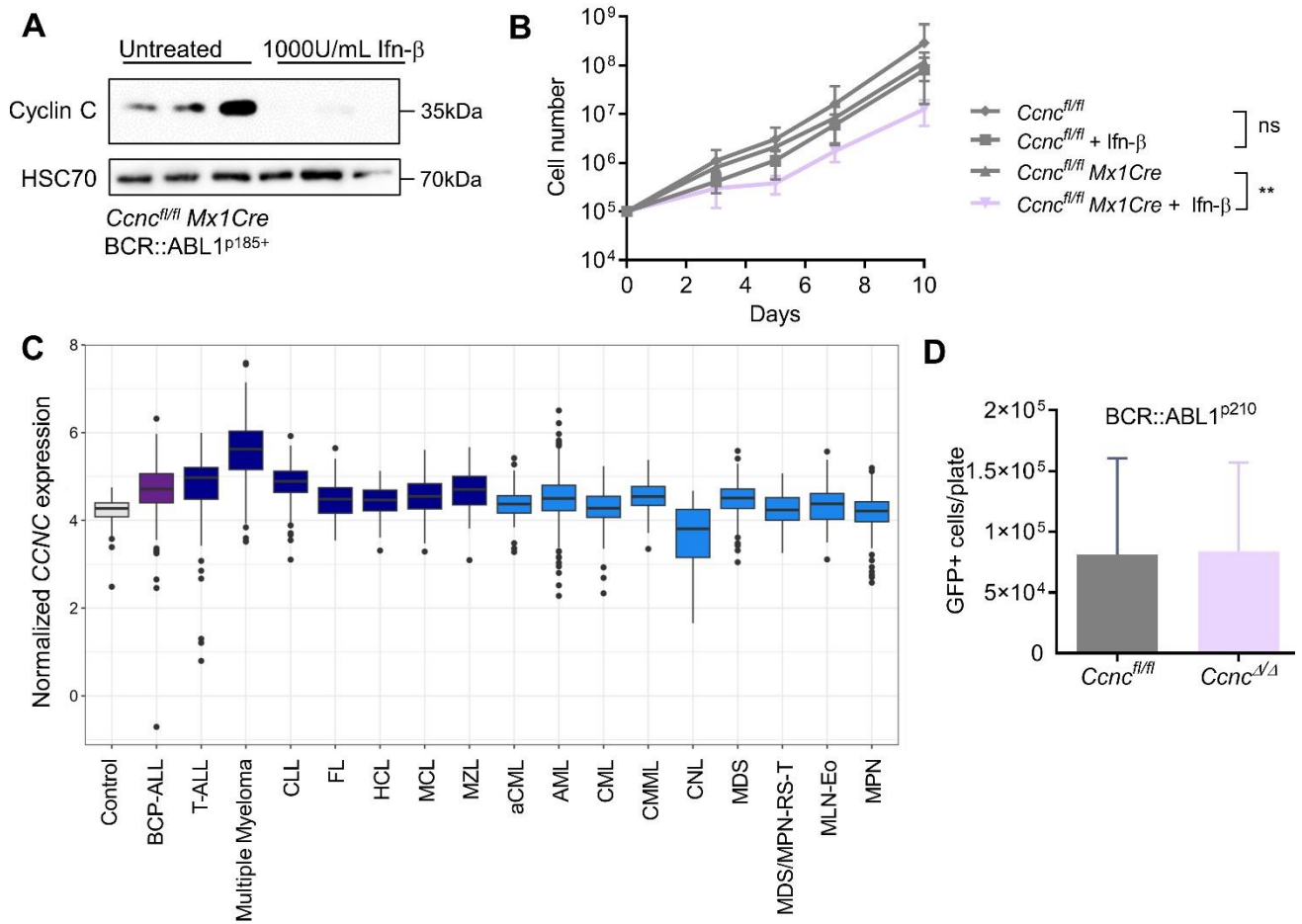


D



Supplementary Figure 6. (A) Immunoblot analysis showing levels of GADD45a, 14-3-3 σ (encoded by *Sfn*) and PLK2 after CRISPR/Cas9 mediated targeting of the respective genes in stable *Ccnc*^{f/f} and *Ccnc* ^{Δ/Δ} BCR::ABL1^{p185+} cell lines in standard culture medium supplemented with 10% FCS. Non-targeting control (sgNTC) or mock treated cells (-) served as control. HSC70 was used as loading control. **(B)** *Ccnc*^{f/f} or *Ccnc* ^{Δ/Δ} BCR::ABL1^{p185+} cells with spontaneous p53 mutations were intravenously injected into NSG mice and survival was monitored. Bar graphs show flow cytometric analysis of BM and spleen infiltration of diseased mice (n = 4 per genotype). **(C)** Cyclin C, p53 and p21 immunoblot analysis of *Ccnc*^{f/f} and *Ccnc* ^{Δ/Δ} BCR::ABL1^{p185+} cell lines infected with dominant negative p53 (dn p53) or empty vector (\emptyset). Cells were treated with DMSO as control or etoposide (1 μ mol/L) for 4 hours to induce p53-dependent p21 expression. HSC70 was used as loading control (n=2 independent cell lines/genotype). **(D)** *Ccnc*^{f/f} + dn p53 or *Ccnc* ^{Δ/Δ} + dn p53 BCR::ABL1^{p185+} cells were intravenously injected into NSG mice and survival was monitored. Bar graph shows infiltration of BCR::ABL1^{p185+} cells in BM and spleens of diseased mice assessed by flow cytometry (n=5 per genotype). Error bars show mean \pm SD. Mann-Whitney U-test was used to calculate levels of significance (B,D). *p < 0.05. Abbreviations: BM, bone marrow; FCS, fetal calf serum

Supplementary Figure 7



Supplementary Figure 7. (A) Immunoblot analysis verifying cyclin C deletion in *Ccnc^{fl/fl} Mx1Cre* BCR::ABL1^{p185+} cells after treatment with 1000U/mL Ifn-β. HSC70 served as loading control (n=3 independent cell lines per genotype). **(B)** *Ccnc^{fl/fl} Mx1Cre* (n=4) cell lines were treated with Ifn-β (1000U/mL) and proliferation was assessed for 10 days. As control, equally treated *Ccnc^{fl/fl}* (n=6) cell lines as well as untreated cell lines (n=4-6/genotype) were used. **(C)** *CCNC* gene expression profile in control (BM mononuclear cells, n=64) vs. patient samples (B-cell precursor acute lymphoblastic leukemia (BCP-ALL): n = 321; T-ALL: n = 136; multiple myeloma: n = 261; chronic lymphocytic leukaemia (CLL): n = 278; follicular lymphoma (FL): n = 63; hairy cell leukemia (HCL), n = 74; mantle cell lymphoma (MCL): n = 83; marginal zone lymphoma (MZL): n= 81; atypical chronic myeloid leukemia (aCML): n = 78; acute myeloid leukemia (AML): n = 743; chronic myeloid leukemia (CML): n = 119; chronic myelomonocytic leukemia (CMML): n = 225; chronic neutrophilic leukemia (CNL): n = 33; myelodysplastic syndrome (MDS): n = 751; MDS/myeloproliferative neoplasm (MPN) with ring sideroblasts and thrombocytosis (MDS/MPN-RS-T): n = 111; myeloid or lymphoid neoplasms associated with eosinophilia (MLN-Eo): n = 46; MPN: n = 259). **(D)** BM from *Ccnc^{fl/fl}* and *Ccnc^{fl/fl} VavCre* mice was isolated and infected with a retrovirus encoding the BCR::ABL1^{p210} oncogene prior to plating in growth-factor free methylcellulose. The number of GFP⁺ cells/plate was determined via flow cytometry after 17 days (n=4/genotype, performed in technical duplicates, one representative result out of two is shown). Error bars depict mean ± SD. Statistical significance was calculated using (B) unpaired t-test on log-transformed counts from day 10 or (D) Mann-Whitney U-test. **p < 0.01. Abbreviations: Ifn-β, interferon beta; BM, bone marrow

Supplementary Materials and Methods

Cell culture maintenance and growth curves

BCR::ABL1^{p185+} cell lines were maintained in RPMI-1640 (Sigma) medium supplemented with 10% fetal bovine serum (FBS; Bio & Sell), 100U/mL penicillin, 100µg/mL streptomycin and 50µM β-mercaptoethanol (Sigma) (RPMI complete medium). The NALM-6 (RRID:CVCL_0092) cell line was kindly provided by Luca Fava (University of Trento, Italy) and cultured in RPMI complete medium supplemented with 10% heat-inactivated FBS. Phoenix-Eco (RRID:CVCL_H717) and A010 Ab-MuLV producer cells were maintained in Dulbecco's Modified Eagle's Medium (DMEM; Sigma) with 10% FBS, 100U/mL penicillin and 100µg/mL streptomycin. For BCR::ABL1^{p185+} growth curves, cells were plated at a density of 10⁵ cells/mL in medium supplemented with 10%FBS. To assess proliferation under stress, cells were seeded with reduced serum (10⁵ cells/mL, 1%FBS) or at a reduced cell density (10⁴/mL, 10%FBS). Cell lines were cultured at 37 °C with 5% CO₂ and regularly tested negative for mycoplasma.

Western Blot analysis

Protein lysates were prepared using SDS lysis buffer or Laemmli lysis buffer. Equal amounts of protein were separated on an 8, 10 or 12% SDS-PAGE gel and transferred to nitrocellulose membranes (Amersham Protran, Merck) or PVDF membranes (Immobilon-P, Merck Millipore) via overnight blotting (0.2mA for 18h followed by 0.4mA for 5h at 4°C) or using a Trans-Blot Turbo System (BioRad). After probing with primary antibodies and incubation with the secondary antibodies (**Supplementary Table S3**), immunoreactive bands were visualized using Clarity Western ECL substrate (BioRad) and the ChemiDoc Touch Imaging System (BioRad).

PCR and qRT-PCR analyses

For comparison of stress responses, BCR::ABL1^{p185+} cells were plated at a density of 10⁵ cells/mL in medium supplemented with 10%FBS. To elicit a stress response, the concentration of FBS was either reduced (1% FCS) or cells were plated at a reduced density (10⁴ cells/mL) for 48 hours prior to RNA isolation. RNA was isolated using the RNeasy Mini Kit (QIAGEN) and reverse transcription was performed using the iScript cDNA Synthesis Kit (Bio-Rad) according to the manufacturer's instructions. The real-time quantitative PCRs (RT-qPCR) were performed using the SsoAdvanced Universal SYBR Green Supermix (Bio-Rad) following the manufacturer's instructions on a CFX96 real-time PCR detection system (Bio-Rad). The qRT-PCR primer sequences are listed in **Supplementary Table S4**. To assess the p53 mutational status, the *Tp53* coding sequence was amplified and Sanger sequenced as previously described¹.

Hemocytometry, histology and microscopy

Blood was collected into EDTA tubes (Mini-Collect K3EDTA Tubes, Greiner Bio-One) from the *vena facialis*. White blood cell (WBC), red blood cell (RBC) and platelet counts were measured using an animal blood counter (scil Vet abc). Blood smears were stained with the Hemacolor Rapid staining of blood smears kit (Sigma-Aldrich). For microscopic images, an Olympus IX71 microscope and the cellSens Dimension software (Olympus) were used.

Flow cytometry and cell sorting

For flow cytometric analysis of primary murine material, single cell suspensions were prepared from bone marrow (BM) and spleen. Blood was collected via puncturing the *vena facialis* and erythrocyte lysis was performed using either red blood cell lysis buffer (10 mM KHCO₃ and 75 mM NH₄Cl, pH 7.4) or BD FACS Lysing Solution (BD Bioscience). The list of antibodies can be found in **Supplementary Table S2**.

Hematopoietic populations were defined as follows: CLP (Lin⁻CD127⁺c-kit^{mid}Sca-1^{mid}CD127⁺); HSC (CD150⁺CD48⁻CD135⁻CD34⁻), MPP1 (CD150⁺CD48⁻CD135⁻CD34⁺), MPP2 (CD150⁺CD48⁺CD135⁻CD34⁺), MPP3 (CD150⁻CD48⁺CD135⁻), and MPP4 (CD150⁻CD48⁺CD135⁺) cell populations gated on Lin⁻Sca-1⁺c-kit⁺ (LSK) cells. For exclusion of Lin⁺ cells, BM was stained with lineage markers (B220, TER119, CD3, Gr-1 and Mac-1). B-cell development populations were defined according to Basel (Hardy/Philadelphia) nomenclature in pre-pro B cells (B220⁺CD43⁺CD19⁻BP-1⁻, fraction A), pro-B (B220⁺CD43⁺CD19⁺BP-1⁻, fraction B), pre-BI/large pre-BII (B220⁺CD43⁺CD19⁺BP-1⁺, fraction C/C'), small pre-BII (B220⁺CD43⁻IgM⁻IgD⁻, fraction D), immature B cells (B220⁺CD43⁻IgM⁺IgD⁻, fraction E), and mature B cells (B220⁺CD43⁻IgM⁺IgD⁺, fraction F)²⁻⁴.

Apoptosis stainings were performed using the Annexin V Apoptosis Detection Kit (eFluor 450, 7-AAD) (ThermoFisher) according to manufacturer's instructions. Cell cycle analysis was performed by staining cells for 30 minutes at 37°C with propidium iodide (PI) staining buffer (0.1% sodium citrate, 0.1% Triton X-100, 100 µg/mL RNase, 20 µg/mL PI). As viability dye, SYTOX Blue Dead Cell Stain (ThermoFisher) was used.

Flow cytometric experiments were performed on a CytoFLEX or CytoFLEX S flow cytometer (Beckman Coulter) and cells were sorted on a BD FACSAria III (BD Bioscience). Data were analysed using CytExpert (version 2.4).

Mouse strains

Conditional *Ccnc*^{fl/fl} mice were kindly provided by Piotr Sicinski⁵ and bred to *VavCre*⁶ and *Mx1Cre*⁷ mice. NSG (NOD.Cg-*Prkdc*^{scid} *Il2rgtm*^{1Wjl}/SzJ; Charles River), *Ccnc*^{fl/fl} *VavCre* (mixed, C57BL/6N × *Sv129*) and *Ccnc*^{fl/fl} *Mx1Cre* (C57BL/6N) mice were bred and maintained under pathogen-free conditions at the University of Veterinary Medicine Vienna, Austria, according to Federation for Laboratory Animal Science Associations (FELASA) guidelines.

Retroviral transductions and establishment of leukemic cell lines

For transformation with the *BCR::ABL1*^{p185+} fusion gene the Phoenix ecotropic packaging system (Phoenix-Eco) and a pMSCV-IRES-GFP retroviral vector containing the *BCR::ABL1*^{p185+} oncogene were used. Briefly, plasmid DNA diluted in serum-free DMEM supplemented with TurboFect (Thermo Fisher Scientific) and 10mM HEPES buffer (pH 7.4) was incubated at room temperature for 15 minutes before dropwise addition to Phoenix-Eco cells (~70% confluency). After incubation for 24 hours at 37°C in a CO₂ incubator, the medium was replaced by the RPMI target cell medium. This viral supernatant was collected 24 and 48 hours later, filtered (0.45µm) and supplemented with 4µg/mL polybrene (Sigma) as well as 10ng/mL interleukin 7 (IL-7; R&D) to infect freshly isolated BM from *Ccnc*^{fl/fl}, *Ccnc*^{fl/fl} *VavCre* or *Ccnc*^{fl/fl} *Mx1Cre* mice. To generate stable *BCR::ABL1*^{p185+} cell lines, cells were then maintained in RPMI complete medium and monitored for outgrowth. Flow cytometric stainings confirmed all outgrowing *Ccnc*^{fl/fl} and *Ccnc*^{ΔΔ} *BCR::ABL1*^{p185+} cell lines as B220+CD19+IgM-IgD- pro-B cells which did not express other lineage markers. An analogous procedure was used for the generation of *BCR::ABL1*^{p185+} cell lines carrying a dominant negative p53 (dn p53) variant by retrovirally infecting stable *BCR::ABL1*^{p185+} cell lines with a pMSCV-dn-p53-IRES-GFP vector or empty vector as control^{8,9}. For *in vitro* deletion of cyclin C in *BCR::ABL1*^{p185+} *Ccnc*^{fl/fl} *Mx1Cre* cell lines, 1000U/mL recombinant mouse interferon-β (IFN-β; Sigma) was added to the cells for 48 hours. Untreated cells and *BCR::ABL1*^{p185+} *Ccnc*^{fl/fl} cells were used as controls. To generate v-abl^{p160+} cell lines, viral supernatant from A010 Ab-MuLV producer cells was harvested, filtered (0.45µm) and supplemented with 4µg/mL polybrene and 10µg/mL IL-7 before infecting *Ccnc*^{fl/fl} and *Ccnc*^{fl/fl} *VavCre* BM.

Colony formation assays

For colony formation assays, BM from gender- and age-matched 6-10 week old *Ccnc*^{fl/fl} or *Ccnc*^{fl/fl} *VavCre* mice was retrovirally transduced with the *BCR::ABL1*^{p185} oncogene as detailed above. For transformation with the *BCR::ABL1*^{p210} fusion gene, a retroviral producer cell line based on the gpE+86 system was used as previously described¹⁰. As control, BM cells were seeded in complete medium. After 24 hours, cells were washed, and equal numbers were seeded in methylcellulose (mouse

methylcellulose base media, R&D Systems) without additional supplements. Another 14-18 days later, colonies were counted and photographed. Cells from BCR::ABL1^{p210+} plates were harvested, washed and counted via FACS. Representative BCR::ABL1^{p185+} colonies were picked, washed, and seeded in RPMI complete medium to monitor outgrowth in liquid culture. For IL-7 dependent colony growth, single cell suspensions were prepared from BM of *Ccnc*^{fl/fl} or *Ccnc*^{fl/fl} *VavCre* mice. The cells were washed, counted and equal numbers embedded in methylcellulose containing 10ng/mL IL-7 (R&D).

RNA Sequencing of BCR::ABL1^{p185+} cell lines

In vitro samples for RNA sequencing were prepared from stable *Ccnc*^{fl/fl} or *Ccnc*^{fl/fl} *VavCre* BCR::ABL1^{p185+} cell lines (n=4). *Ex vivo* samples were generated by injecting the same cell lines into gender-matched, 11 week old NSG mice (5x10⁵ cells injected i.v. via tail vein). For retrieval of BCR::ABL1^{p185+} cells ten days after injection, living (Sytox Blue-negative) Ly5.1⁻CD19⁺GFP⁺ cells were sorted. A total of 4x10⁵-1x10⁶ *Ccnc*^{fl/fl} BCR::ABL1^{p185+} cells and 2.2x10⁵ *Ccnc*^{Δ/Δ} were sorted from the BM. Total RNA was extracted using the RNeasy Micro Kit (QIAGEN). The RNA was subjected to library prep for next generation sequencing (NGS) with Illumina technology using the SmartSeq3 protocol¹¹ and Nextera adapters. Sequencing was performed on an Illumina NovaSeq Instrument (Illumina, San Diego, CA, USA), using an S4 flowcell with paired-end mode, sequencing 150 bp per read. Raw reads were quality controlled using Fastqc version 0.11.9. Trimmomatic version 0.39¹² was used to filter reads and umi-tools version 1.1.1¹³ was used to remove unique molecular identifier sequences. The reads were then aligned against the GRCm38 primary assembly mouse reference genome using STAR version 2.7.6a with the "Gencode M25 primary assembly annotation" gene model^{14,15}. Reads covering exons were counted using the featureCounts program¹⁶ from the Subread package version 2.0.1¹⁷ and total counts were reported at the gene level for each sample in form of a count matrix. Further quality control by assessing fraction of reads assigned to genes, by comparison of count distributions and by principal component analysis identified 5/16 samples to be of low quality. These samples were excluded from further analysis. Differential gene expression was analyzed with R version 4.0.3 using RStudio version 1.3.1093 and the DESeq2 package version 1.30.0¹⁸⁻²⁰. The RNA-Seq data reported in this article have been deposited in the Array Express database (accession number: E-MTAB-13728).

Gene set enrichment analysis (GSEA)

For GSEA, ranked gene lists were prepared from the results of the differential gene expression analysis^{21,22}. We used $\text{sign}(\log_2\text{FoldChange}) * (-1) * \log_{10}(\text{p-value})$ as the rank metric for each gene ("log₂FoldChange" and "p-value" were taken from the DESeq2 results object). GSEA was then performed using the GSEA software (version 4.1.0). Enrichment of gene set collections from MSigDB

(version 7.2) was tested^{23,24}. The analysis was performed using the command-line script and the “GSEAPreranked” analysis mode. To map mouse ensembl gene IDs to human gene symbols we used the gene annotation chip-file provided with MSigDB after removal of duplicate mappings. The “collapse” parameter was set to “Remap_Only” and the “scoring_scheme” parameter to “classic”.

DepMap Analysis

Genetic dependency analyses in a panel of tumor cell lines were performed using the DepMap platform (<https://depmap.org/portal/>, accessed on 8.11.2023) and the most recent DepMap CRISPR database (Depmap Public 23Q2+Score, Chronos)^{25–28}.

CRISPR/Cas9 mediated knock-out cell lines

Knock-out NALM-6 cells were generated using direct delivery of the CRISPR/Cas9 system as previously described²⁹ with a ribonucleoprotein (RNP) complex consisting of Cas9 protein and guide RNAs (gRNAs) targeting *HPRT1* (GCATTTCTCAGTCCTAAACA) or one of three guides targeting *CCNC* (TAGGCAAAGATCCGTTCTGT, GGCCCATGTCCTGCACATAC and TCTGTTGAAGGAGCGCCAAA). Briefly, crRNA (100µM, IDT) and tracrRNA (100µM, IDT) were annealed in equimolar concentrations to form gRNAs. For a total of 2x10⁵ NALM-6 cells, 120pmol recombinant Cas9 (IDT) were complexed with 150pmol of the respective gRNA for RNP formation. Electroporation was performed using Lonza Nucleofector 4D according to manufacturer’s instructions and 4µM electroporation enhancer (100µM, IDT). Monoclonal cell lines were generated in 96-well plates through limiting dilution, or by seeding single cells with a BD FACSAria III (BD Bioscience) cell sorter. An analogous procedure was used for CRISPR/Cas9 mediated gene editing in BCR::ABL1^{p185+} cell lines using Lonza Nucleofector 2b with 1µM electroporation enhancer and 1x10⁶ cells. Two different gRNAs per gene were pooled to target *Gadd45a* (CTCGTACACGCCGACCGTAA, GGCACAGTACCACGTTATCG), *Sfn* (GTAGCTTACAAGAACGTGGT, TTCCGTAGCTTACAAGAACG) or *Plk2* (TTATAGTCGACCCACGACG, ACGAACAAGAAATCTTGCAC). Assays were performed 6 days after direct delivery of the respective RNP complex.

Data Visualization and Statistical Analysis

Data were visualized and analyzed using R version 4.3.2¹⁸ with RStudio version 2023.09.1¹⁹ or GraphPad Prism version 8.4.3 for Windows (GraphPad Software, San Diego, California USA, www.graphpad.com). Statistical significance was calculated using the appropriate statistical method as indicated in the corresponding Figure Legends. CoreIDRAW Graphics Suite (version 23.0.0.363) was used for some graphical illustrations.

Supplementary Tables

Supplementary Table S1. Differentially expressed p53 hallmark genes.

Differentially expressed genes (padj<0.1) in the p53 hallmark mouse gene set^{21,23,24,30,31} between *Ccnc*^{Δ/Δ} vs. *Ccnc*^{fl/fl} BCR::ABL1^{p185+} cells after retrieval from BM of NSG mice (“*ex vivo*” samples) 10 days post-injection, sorted by log2 fold-change.

Gene	ID	log2 (fold-change)	padj
<i>Ptpn14</i>	ENSMUSG00000026604.17	5.09	3.54E-06
<i>Cdkn2a</i>	ENSMUSG00000044303.6	2.89	6.45E-02
<i>Ndrp1</i>	ENSMUSG00000005125.13	2.88	5.14E-03
<i>Rgs16</i>	ENSMUSG00000026475.7	2.33	7.26E-04
<i>Ier3</i>	ENSMUSG00000003541.6	1.95	6.49E-02
<i>Cdkn2b</i>	ENSMUSG00000073802.5	1.92	1.42E-03
<i>Stom</i>	ENSMUSG00000026880.11	1.87	1.10E-02
<i>Tcn2</i>	ENSMUSG00000020432.12	1.82	1.07E-02
<i>Gadd45a</i>	ENSMUSG00000036390.8	1.78	2.85E-03
<i>Btg1</i>	ENSMUSG00000036478.8	1.74	1.11E-08
<i>Plk2</i>	ENSMUSG00000021701.8	1.74	3.57E-02
<i>Pitpnc1</i>	ENSMUSG00000040430.18	1.39	8.47E-02
<i>Ccnd2</i>	ENSMUSG00000000184.12	1.27	6.91E-04
<i>Sfn</i>	ENSMUSG00000047281.3	1.20	3.64E-02
<i>Tspyl2</i>	ENSMUSG00000041096.13	1.15	1.91E-02
<i>Mxd4</i>	ENSMUSG00000037235.13	0.99	1.98E-03
<i>Tgfb1</i>	ENSMUSG00000002603.15	0.94	2.73E-04
<i>Rap2b</i>	ENSMUSG00000036894.3	0.94	3.76E-02
<i>Casp1</i>	ENSMUSG00000025888.6	0.92	6.29E-02
<i>Mxd1</i>	ENSMUSG00000001156.9	0.87	6.10E-02
<i>Btg2</i>	ENSMUSG00000020423.6	0.86	4.83E-03
<i>Cd82</i>	ENSMUSG00000027215.13	0.78	7.13E-02
<i>Epha2</i>	ENSMUSG00000006445.3	0.75	1.33E-02
<i>Hras</i>	ENSMUSG00000025499.18	0.75	3.48E-02
<i>Gm2a</i>	ENSMUSG00000000594.7	0.71	4.16E-02
<i>Iscu</i>	ENSMUSG00000025825.12	0.67	3.42E-03
<i>Tap1</i>	ENSMUSG00000037321.17	0.65	7.15E-02

<i>Rab40c</i>	ENSMUSG00000025730.14	0.65	8.02E-02
<i>Rchy1</i>	ENSMUSG00000029397.15	0.60	4.65E-02
<i>Def6</i>	ENSMUSG00000002257.8	0.50	7.87E-02
<i>Fam162a</i>	ENSMUSG00000003955.8	-0.66	1.03E-03
<i>Steap3</i>	ENSMUSG00000026389.16	-0.69	1.37E-02
<i>Cdkn1a</i>	ENSMUSG00000023067.14	-0.71	8.43E-02
<i>Hint1</i>	ENSMUSG00000020267.6	-0.81	1.73E-04
<i>Rpl36</i>	ENSMUSG00000057863.6	-0.97	2.21E-06
<i>Rps27l</i>	ENSMUSG00000036781.13	-0.98	2.82E-04
<i>Tprkb</i>	ENSMUSG00000054226.13	-1.01	6.27E-04
<i>H2aj</i>	ENSMUSG00000060032.6	-1.08	1.28E-05
<i>Sdc1</i>	ENSMUSG00000020592.14	-1.08	8.63E-02
<i>Rpl18</i>	ENSMUSG00000059070.16	-1.09	1.82E-05
<i>Mknk2</i>	ENSMUSG00000020190.13	-1.09	4.31E-05
<i>Hlf2</i>	ENSMUSG00000036181.2	-1.13	3.05E-05
<i>Pcna</i>	ENSMUSG00000027342.14	-1.20	1.41E-07
<i>Ada</i>	ENSMUSG00000017697.3	-1.28	9.91E-05
<i>Pmm1</i>	ENSMUSG00000022474.15	-1.40	1.26E-05
<i>Rack1</i>	ENSMUSG00000020372.15	-1.46	2.33E-08
<i>Rps12</i>	ENSMUSG00000061983.7	-1.58	5.27E-12

padj, Benjamini-Hochberg adjusted p-value

Supplementary Table S2. Flow cytometric antibodies.

Target	Conjugate	Clone	Company	Cat. No.
CD19	APC-Cy7	1D3	BD Biosciences	557655
	FITC	1D3	Biolegend	152404
	eFluor 450	eBIO1D3	eBioscience	48-0193
B220 (CD45R)	PerCP-Cy5.5	RA3-6B2	BD Biosciences	552771
	APC-eFluor780	RA3-6B2	eBioscience	47-0452
CD43	PE	S7	BD Biosciences	553271
CD3	Pacific Blue	17A2	BioLegend	100214
	APC-eFluor780	17A2	eBioscience	47-0032
CD11b	APC-Cy7	M1/70	BD Biosciences	557657
BP-1 (CD249)	Biotin	6C3	eBioscience	13-5891
	APC-Cy7		Biolegend	405208
Streptavidin	eFluor 450		eBioscience	48-4317
	Brilliant Violet 650		Biolegend	405231
IgM	FITC	II/41	eBioscience	11-5790
	Biotin	II/41	eBioscience	13-5790
IgD	APC	11-26	eBioscience	17-5993
Ter119	APC-eFluor 780		eBioscience	47-5921
Ly-6G/Ly-6C (Gr-1)	APC-Cy7	RB6-8C5	Biolegend	108424
	APC-eFluor780	RB6-8C5	eBioscience	47-5931
CD48	PE	HM48-1	eBioscience	12-0481
CD150	Brilliant Violet 510	TC15-12F12.2	Biolegend	115929
CD34	FITC	RAM34	BD Biosciences	553733
CD135	Biotin	A2F10	Biolegend	135308
Sca-1 (Ly6A/E)	PE-Cy7	D7	BD Pharmingen	558162
c-kit (CD117)	PE-Cyanine5	2B8	eBioscience	15-1171
CD127	eFluor 450	A7R34	eBioscience	48-1271

Supplementary Table S3. Immunoblotting antibodies.

Target	Cat. No.	Company
HSC70 (B-6)	sc-7298	Santa Cruz
Cyclin C	A301-989A	Bethyl
CDK8 (G398)	#4101	Cell Signaling
CDK19	HPA007053	Sigma-Aldrich
p53	sc-393031	Santa Cruz
p21	sc-6246	Santa Cruz
p16INK4a	ab211542	Abcam
p19ARF	ab80	Abcam
Cyclin D2	sc-593	Santa Cruz
NDRG1	26902-1-AP	Proteintech
PLK2	15956-1-AP	Proteintech
GADD45a	#4632	Cell Signaling
14-3-3 Sigma	10622-1-AP	Proteintech/Thermo Fisher
Anti-mouse IgG, HRP-linked	#7076	Cell Signaling
Anti-rabbit IgG, HRP-linked	#7074	Cell Signaling

Supplementary Table S4. qRT-PCR primers.

Gene	Forward (5'>3')	Reverse (5'>3')
<i>Actb</i>	CTCTGGCTCCTAGCACCATGAAGA	GTAAAACGCAGCTCAGTAACAGTCCG
<i>Rplp0</i>	GCTTTCTGGAGGGTGTCC	GCTTCAGCTTTGGCAGGG
<i>Cdkn2b</i>	CCCTGCCACCCTTACCAGA	CAGATACCTCGCAATGTCACG
<i>Cdkn1a</i>	GAACATCTCAGGGCCGAAA	ATCTGCGCTTGGAGTGATAG
<i>Gadd45a</i>	CTGCAGAGCAGAAGACCGAA	GGGTCTACGTTGAGCAGCTT
<i>Plk2</i>	GAGCCTCCTCCGGACAAAA	GAGCCGAGGTCTTCGAATGT
<i>Sfn</i>	TCTGATCCAGAAGGCCAAGT	CCCACCACGTTCTTGTAAGC

Supplementary References

1. Bellutti F, Tigan AS, Nebenfuehr S, et al. CDK6 antagonizes P53-induced responses during tumorigenesis. *Cancer Discov* 2018;8(7):884–897.
2. Hardy RR. B-cell commitment: Deciding on the players. *Curr Opin Immunol* 2003;15(2):158–165.
3. Hardy RR, Li Y-S, Allman D, Asano M, Gui M, Hayakawa K. B-cell commitment, development and selection. *Immunol Rev* 2000;175(1):23–32.
4. Rolink A, Melchers F. Molecular and cellular origins of B lymphocyte diversity. *Cell* 1991;66(6):1081–1094.
5. Li N, Fassl A, Chick J, et al. Cyclin C is a haploinsufficient tumour suppressor. *Nat Cell Biol* 2014;16(11):1080–1091.
6. Georgiades P, Ogilvy S, Duval H, et al. VavCre transgenic mice: a tool for mutagenesis in hematopoietic and endothelial lineages. *Genesis* 2002;34(4):251–256.
7. Kühn R, Schwenk F, Aguet M, Rajewsky K. Inducible gene targeting in mice. *Science* 1995;269(5229):1427–1429.
8. Schuster C, Berger A, Hoelzl MA, et al. The cooperating mutation or “second hit” determines the immunologic visibility toward MYC-induced murine lymphomas. *Blood* 2011;118(17):4635–4645.
9. Shaulian E, Zauberman A, Ginsberg D, Oren M. Identification of a Minimal Transforming Domain of p53: Negative Dominance through Abrogation of Sequence-Specific DNA Binding. *Mol Cell Biol* 1992;12(12):5581–5592.
10. Sexl V, Piekorz R, Moriggl R, et al. Stat5a/b contribute to interleukin 7-induced B-cell precursor expansion, but abl- and bcr/abl-induced transformation are independent of Stat5. *Blood* 2000;96(6):2277–2283.
11. Hagemann-Jensen M, Ziegenhain C, Chen P, et al. Single-cell RNA counting at allele and isoform resolution using Smart-seq3. *Nat Biotechnol* 2020 386 2020;38(6):708–714.
12. Bolger AM, Lohse M, Usadel B. Trimmomatic: a flexible trimmer for Illumina sequence data. *Bioinformatics* 2014;30(15):2114–2120.
13. Smith T, Heger A, Sudbery I. UMI-tools: modeling sequencing errors in Unique Molecular

- Identifiers to improve quantification accuracy. *Genome Res* 2017;27(3):491–499.
14. Frankish A, Diekhans M, Ferreira AM, et al. GENCODE reference annotation for the human and mouse genomes. *Nucleic Acids Res* 2019;47(D1):D766–D773.
 15. Dobin A, Davis CA, Schlesinger F, et al. STAR: ultrafast universal RNA-seq aligner. *Bioinformatics* 2013;29(1):15–21.
 16. Liao Y, Smyth GK, Shi W. featureCounts: an efficient general purpose program for assigning sequence reads to genomic features. *Bioinformatics* 2014;30(7):923–930.
 17. Liao Y, Smyth GK, Shi W. The Subread aligner: Fast, accurate and scalable read mapping by seed-and-vote. *Nucleic Acids Res* 2013;41(10):e108.
 18. R Core Team. R: A Language and Environment for Statistical Computing. *R Foundation for Statistical Computing, Vienna, Austria*.
 19. RStudio Team. RStudio: Integrated Development Environment for R (RStudio, PBC, Boston, MA). 2020;URL:<http://www.rstudio.com>.
 20. Love MI, Huber W, Anders S. Moderated estimation of fold change and dispersion for RNA-seq data with DESeq2. *Genome Biol* 2014;15(12):1–21.
 21. Subramanian A, Tamayo P, Mootha VK, et al. Gene set enrichment analysis: A knowledge-based approach for interpreting genome-wide expression profiles. *Proc Natl Acad Sci U S A* 2005;102(43):15545–15550.
 22. Mootha VK, Lindgren CM, Eriksson KF, et al. PGC-1 α -responsive genes involved in oxidative phosphorylation are coordinately downregulated in human diabetes. *Nat Genet* 2003;34(3):267–273.
 23. Liberzon A, Subramanian A, Pinchback R, Thorvaldsdóttir H, Tamayo P, Mesirov JP. Molecular signatures database (MSigDB) 3.0. *Bioinformatics* 2011;27(12):1739–1740.
 24. Liberzon A, Birger C, Thorvaldsdóttir H, Ghandi M, Mesirov JP, Tamayo P. The Molecular Signatures Database (MSigDB) hallmark gene set collection. *Cell Syst* 2015;1(6):417.
 25. Meyers RM, Bryan JG, McFarland JM, et al. Computational correction of copy number effect improves specificity of CRISPR-Cas9 essentiality screens in cancer cells. *Nat Genet* 2017;49(12):1779–1784.

26. Dempster JM, Boyle I, Vazquez F, et al. Chronos: a cell population dynamics model of CRISPR experiments that improves inference of gene fitness effects. *Genome Biol* 2021;22(1):1–23.
27. Pacini C, Dempster JM, Boyle I, et al. Integrated cross-study datasets of genetic dependencies in cancer. *Nat Commun* 2021;12(1):1–14.
28. Dempster JM, Rossen J, Kazachkova M, et al. Extracting Biological Insights from the Project Achilles Genome-Scale CRISPR Screens in Cancer Cell Lines. *bioRxiv* 2019;720243.
29. Ghetti S, Burigotto M, Mattivi A, et al. CRISPR/Cas9 ribonucleoprotein-mediated knockin generation in hTERT-RPE1 cells. *STAR Protoc* 2021;2(2):100407.
30. Castanza AS, Recla JM, Eby D, Thorvaldsdóttir H, Bult CJ, Mesirov JP. Extending support for mouse data in the Molecular Signatures Database (MSigDB). *Nat Methods* 2023;20(11):1619–1620.
31. Howe DG, Blake JA, Bradford YM, et al. Model organism data evolving in support of translational medicine. *Lab Anim (NY)* 2018;47(10):277–289.